LIGHT REFLECTANCE SPECTROSCOPY FOR THE DETECTION OF POSITIVE SURGICAL MARGIN OF PROSTATE CANCER

By

Henry Chan

A THESIS SUBMITTED IN PARTIAL FULFILLMENT OF THE REQUIREMENTS FOR

THE DEGREE OF

MASTER OF SCIENCE

BIOMEDICAL ENGINEERING

UNIVERSITY OF TEXAS AT ARLINGTON

JOINT PROGRAM WITH THE UROLOGY DEPARTMENT AT THE UNIVERSITY OF TEXAS SOUTHWESTERN MEDICAL CENTER

MAY 2017

Acknowledgements

It has been a long journey from when I first became a graduate student at the University of Texas at Arlington (UTA) in the fall of 2015. I first met Dr. Hanli Liu, PhD., Professor in Bioengineering, University of Texas at Arlington, when I was discussing my future in terms of the different track programs offered here at UTA. I could immediately tell that Dr. Liu was very knowledgeable, and I was impressed by the effort and time she spent on her students. It was then I knew I wanted Dr. Liu to become my mentor. I enrolled into one of her courses in an effort to be acknowledged and considered as her future Graduate Research Assistant (GRA). Dr. Liu's teaching style immediate showed me what kind of professor she is. She genuinely wants her students to learn, and she takes time out of her busy schedule to ensure the success of all of her students. Dr. Liu is one of two professors at UTA that I truly respect in terms of teaching style, student involvement, and character. I entered her lab with zero experience in research and was very intimidated by the research field when I first began. But Dr. Liu understands how new students in research feel. She told a story of her past where she too was once new to the research field, and she understands how to properly train her students. She truly nurtured and guided me into the experienced researcher I am today. I am thoroughly grateful for her and her efforts in supporting her students and allowing them a chance to grow both professionally and as a person. The opportunities I have gained through Dr. Liu's lab are invaluable. I have gained many friends and colleagues throughout my journey working as a GRA in Dr. Liu's lab and at the University of Texas Southwestern campus. These memories, I will cherish forever. Thank you for everything Dr. Liu.

In addition, I would like to acknowledge Dr. Jeffrey Cadeddu, MD., Professor of Urology and Radiology, University of Texas Southwestern Medical Center. Dr. Cadeddu is the founder of this project in the use of Light Reflectance Spectroscopy for the Detection of Positive Surgical Margins of Prostate Cancer. He made it possible for me to explore the experiences I gained in clinical research. I would like to thank Dr. Cadeddu for giving me this opportunity, funding my research, and providing me with skills and experiences that I will take into my future. I also would like to acknowledge Dr. Payal Kapur, MD., Associate Professor of Pathology and Urology, University of Texas Southwestern Kidney Cancer Program and Co-Leader in Pathology. Dr. Kapur has allowed me to have regular access to her pathology lab in order to perform my measurements for my research. I would like to thank her for taking time from her very busy schedule and performing time consuming pathology analysis on the prostate tissue specimens I have measured. I would also like to acknowledge Dr. Claus G. Roehrborn, MD., Professor and Chair of the Department of Urology at the University Of Texas Southwestern Medical Center. Dr. Roehrborn has played a key role in this research in the past and he has allowed me to perform research on many of his prostate cases in which he has performed prostatectomies. I would also like to acknowledge Dr. Igor Sorokin, MD., Fellow of Urology and Radiology, University of Texas Southwestern Medical Center. Igor has been excellent in collaborating and coordinating between the pathology reports, LRS reports, and providing the medical knowledge necessary for the success of this research.

I would also like to acknowledge my lab mates Xinlong Wang, PhD. Candidate, University of Texas at Arlington. Thank you Xinlong for training me, advising me, and providing the utmost assistance in ensuring my success in research. He is as much as a second mentor, but a good friend. I wish success to him and his family in the future. And I would like to acknowledge Chandan Bangalore

for assisting me in the technical realms of programing and spending many hours in redesigning my algorithms in an effort to save time and improve efficiency of my work.

To all, thank so very much for contributing to this work and providing me with unforgettable memories and experiences in research for the detection of positive surgical margins of prostate cancer, using Light Reflectance Spectroscopy. It has truly been a journey.

May 9, 2017

Abstract

LIGHT REFLECTANCE SPECTROSCOPY FOR THE DETECTION OF POSITIVE SURGICAL MARGIN OF PROSTATE CANCER

Henry Chan, MS

The University of Texas at Arlington, 2017

During a radical prostatectomy in the operating room, there exists a certain degree of risks of a surgical positive margin of prostate cancer. Positive surgical margins are defined as cancer that has spread beyond the margin of the prostate and into the surrounding tissues. Surgeons will be able to utilized the concept of Light Reflectance Spectroscopy (LRS) in real-time during surgery to help detect these positive surgical margins and to provide the surgeon a quantitative decision to remove the excess surrounding tissues. This modality would essentially lower the risks of positive surgical margins and prevent the recurrence of cancer, effectively improving the survival of the patient. LRS is highly dependent on the Gleason Score (GS) of the cancer. Based off the 5 and 9 Feature Algorithm, select features of the spectral curve are used to differentiate between normal tissue and cancerous tissue. It is most effective in distinguishing between normal tissue versus high grade cancers such as GS 4+3 and GS 4+4, primarily due to the Gleason Grade 4 pattern. But LRS is less effective in distinguishing lower grade cancers such as GS 6 (3+3) and GS 3+4, primarily due to the Gleason Grade 3 pattern. The 5 Feature Algorithm is the current optimal form of cancer classification algorithm for higher grade cancers, with a Sensitivity and Specificity value of 72.2% and 81.5%, respectively, for the GS 4+4 groups. In addition, there is a question if applying an excess level of pressure onto the surface of the prostate using the optical probe would affect the spectral readings of the LRS measurement. It was found that applying pressures up to ~0.066

N/mm^2 does not significantly affect the spectral readings at a peak wavelength value of 630 nm. Also, two new optical probes, a new 370 µm probe and a new 125 µm, were introduced into the study and the penetration depths were calculated. It was found that the new 370 µm probe had a penetration depth range from 1.77 mm to 1.95 mm. The new 125 µm probe had a penetration depth range from 1.06 mm to 1.41 mm.

Table of Contents

Chapter 1: Introduction

1.1 What is the Prostate?

The prostate is a gland found only in males and is responsible for secreting fluid that helps nourishes and protects sperm cells and is release during ejaculation as sperm. The prostate gland is approximately the size of a walnut and is located below the bladder and above the penis. The urethra runs through the prostate and connects the bladder to the penis to allow the flow of urine during micturition. [1]

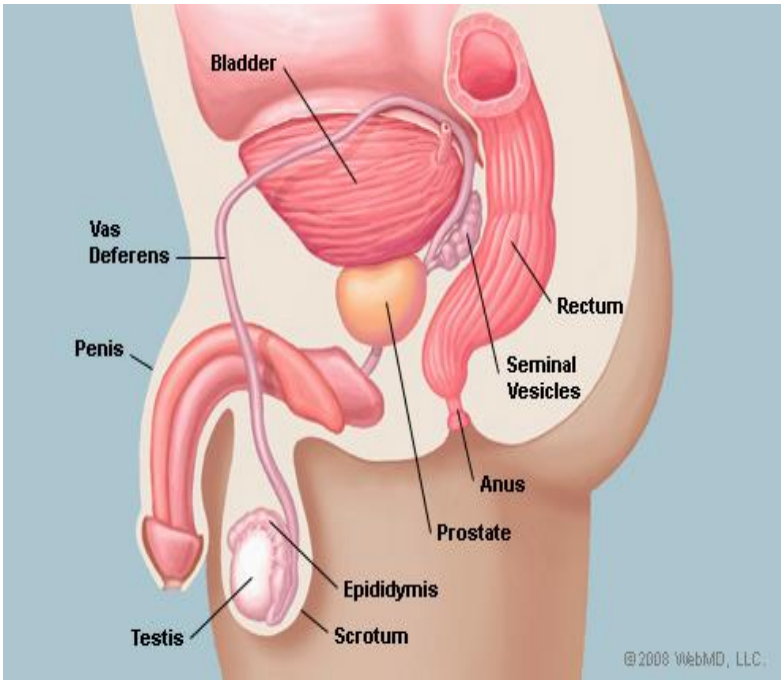

Figure 1: A schematic of the male anatomy, displaying the location of the prostate organ. [2]

1.2 What is Prostate Cancer?

After skin cancer, prostate cancer is the most common form of cancer in men. Cancer is a disease where cells grow and proliferate at an uncontrollable rate. It possess serious risks due to its ability to spread and invade other areas of the body. Prostate cancer generally begins when the cells of the prostate proliferate uncontrollably, often times forming into a mass called a tumor. Prostate cancers are usually slow growing, but in some cases, it can grow and spread at a faster pace. [2]

There are several types of prostate cancer, but the vast majority of prostate cancers are adenocarcinomas. Adenocarcinomas are cancers that develop from the gland cells of the prostate. These gland cells are responsible for producing nourishing prostate fluid that is combined with sperm to form semen. Other forms of prostate cancers include sarcomas, small cell carcinomas, neuroendocrine tumors, and transitional cell carcinomas. [2]

The American Cancer Society estimates that for the year 2017 in the United States, there will be approximately 161,360 new cases of prostate cancer and approximately 26,730 deaths that results from prostate cancer. Approximately 1 in 7 men will be diagnose in his lifetime with prostate cancer, primarily affecting older men aged 65 or older. The average age for men diagnosed with prostate cancer is roughly 66 years old. Approximately 1 out of 39 men diagnosed with prostate cancer will die. [3]

1.3 Gleason Score and Cancer Classification

Gleason score is a method to classify the grade of the prostate cancer and to rank the progression of the cancer. Pathologists are responsible for grading the prostate cancer and assign a grade

from 1 to 5 based on the type of tissue they observe using a microscope. Grade 1 is assigned for cancerous tissue that looks very similar to normal prostate tissue. Grade 5 is assigned for cancerous tissue that has very abnormal growth patterns and features that are characteristic of cancer. Grades 2 to 4 are assigned to tissue that have intermediate characteristics between the Grades 1 and 5 extremes. Grades 1 and 2 are usually not used for biopsies due to its very low risk factor. [4]

Prostate cancer often times have different grades in different areas. A grade, from 1 to 5, will be assigned to each of the two areas, which makes up the majority of the cancerous areas. The two grades are added into the Gleason Score, also known as Gleason Sum. The first number reported will represent the most common grade in the tumor by volume. And the second grade represents the least common grade in the tumor by volume. As an example, a Gleason score of 3+4 = 7 means that the majority of the tumor is grade 3, and the minority of the tumor is grade 4. These scores are added to produce a Gleason score of 7. [4]

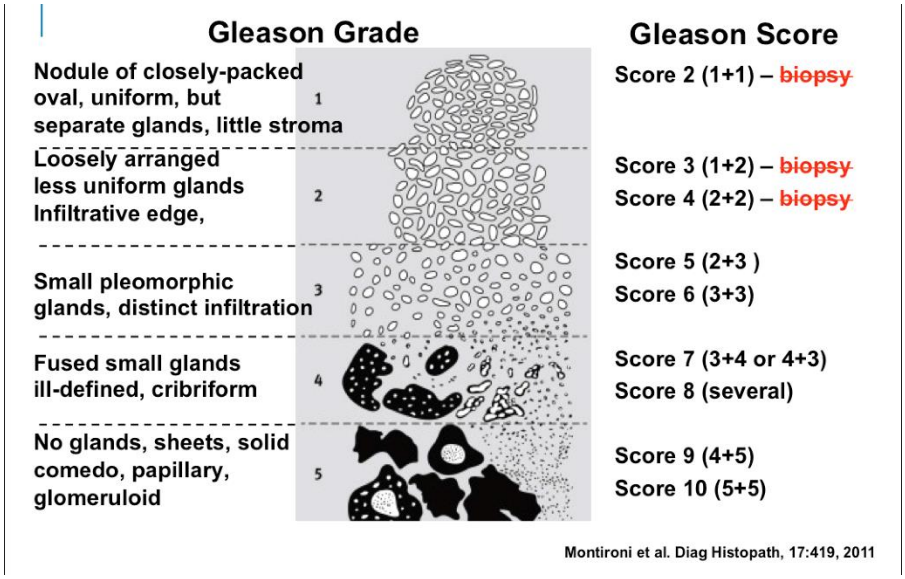

Figure 2: A schematic summarizing the Gleason Grades and Gleason Score based off tissue and cell properties. [16]

1.4 Current Prostate Cancer Diagnosis Tools

The most common initial diagnosis of an organ-confined prostate involves a Digital Rectal Examination (DRE). The physician evaluates the size, shape, and texture of the prostate by inserting his/her digit into the rectum. [3] A blood test is also performed to determine the Prostate Specific Antigen (PSA) levels. PSA levels are age-specific, usually levels above 4 ng/mL are considered suspicious for cancer and may lead to a prostate biopsy. However, PSA test is not a perfect testing tool for prostate cancer. Men with PSA levels between the age specific levels and 10 ng/mL may not actually have prostate cancer. Higher levels of PSA may result from other factors, other than cancer. Such as benign prostatic hyperplasia (BPH) or prostatitis. In general, the larger the size of the prostate, the higher the level of PSA in the blood. [3]

Prostate biopsies are performed after a suspicious DRE test and/or abnormally high levels of PSA. Prostate biopsies confirm these findings by obtaining small samples from 6-12 regions of the prostate. These samples are removed by a biopsy gun equipped with a needle which penetrates the prostate via the rectum. The samples are observed by a pathologist under a microscope, and prostate cancer diagnosis can be confirmed. [3] Biopsy test results samples less than 1% of the prostate volume and may lead to missing significant prostate cancer detection. On the contrary, a positive biopsy may detect a non-life-threatening cancer and may lead to over-treatment, usually the complete removal of the prostate via radical prostatectomy. [3]

1.5 Current Prostate Cancer Treatment Tools

A man diagnosed positive for prostate cancer has a variety of options for treatment. The major forms of treatments include active surveillance, radiation, and surgery. There are also other

nonstandard treatment options which include cryotherapy, high-intensity focused ultrasound, and hormone therapy. [4]

Active Surveillance is a form of treatment that involves careful monitoring of the progression of prostate cancer. DRE and PSA are usually performed periodically. After a year, a prostate biopsy is performed and then repeated at a specific time interval. The physician monitors the patient for symptoms, and if symptoms develop, further aggressive treatments may be necessary. [5]

Radiation is a form of treatment that kills cancer cells and the surrounding tissue using radioactive exposure. There are three major types of radiation: External Beam Radiation Therapy (EBRT), Proton Therapy (PT), and Brachytherapy (BT). EBRT is the most common form of radiation therapy. CT scans and MRIs are often used to create a map and localize the tumor cells. X-rays then target and radiates the cancer cells using 3-D conformal radiotherapy which precisely kills cancer cells using the highest dosage of radiation. [6]

PT is another form of radiotherapy, and has higher precision than EBRT. PT uses photon particles to target cancer cells without damaging the surrounding tissue. However, PT is very expensive, with very few medical institutions that can afford such equipment. [6]

BT is the third major form of radiotherapy. BT makes use of tiny metal pellets, infused with radioactive iodine or palladium, which are inserted into the organ-confined prostate using needles. Over time, radiation is released by the seeds to the immediate surrounding tissue, effectively killing the surrounding cancer cells. [6]

Surgery is the third major form of treatment, in most cases, the entire prostate is removed. Men will undergo Radical Prostatectomy (RP), the removal of the entire prostate and some

surrounding tissue. Men with more advanced progression of prostate cancer may also have their lymph nodes removed. The most common form of RP is robotic radical prostatectomy (RRP). In RRP, small incisions are made in the abdomen and a robotic interface is used to maneuver a robotic arm, equipped with cameras and instruments, to remove the prostate gland. [7]

In RP, the surgeon has the option to preserve the erectile nerves that run along the capsule of the prostate, termed nerve-sparing prostatectomy (NSP). The surgeon will not know if he will perform NSP until the time of the procedure. If the cancer has invaded the surrounding nerve tissue, NSP is not often times not possible. NSP offers the patients long-term erectile function. [7]

1.6 Positive Surgical Margins

During RP, the surgeon's objective is to remove the prostate gland and remove just enough surrounding tissue to ensure the complete remove of the cancer. Often times, the surgeon will aim to preserve the erectile nerve tissue, however, there needs to be a precise balance between preserving erectile nerve tissue and removing surrounding cancerous tissue. When a pathologists examines the prostate tissue, he may observe cancerous tissue at the capsule of the prostate tissue. This may imply that the cancer has invaded beyond the prostate gland and into the surrounding tissue. There is a high possibility that cancer was left behind inside the patient. Positive surgical margins likelihood increases with extracapsular extension, when the cancerous cells invade beyond the prostate capsule and into the surrounding tissue. Surgeons must pay particular attention to this and perform wider cuts around the prostate to ensure the complete removal of the cancer. [8]

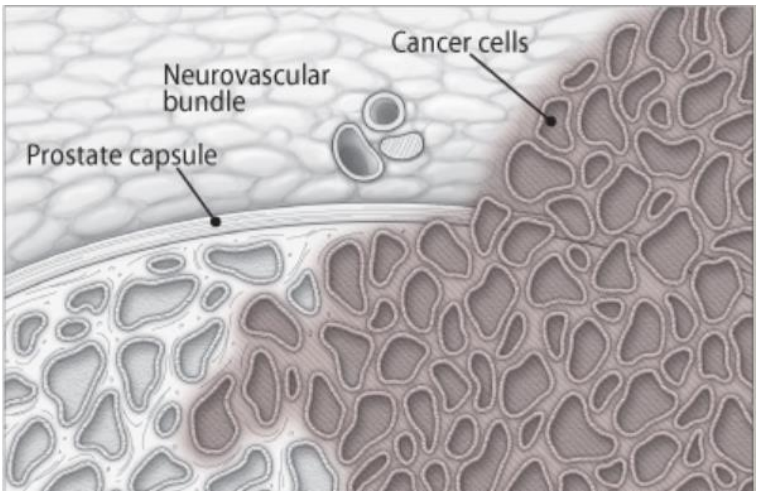

Figure 3: A schematic representing a positive surgical margin of cancer cells invading beyond the margins of the prostate capsule. [8]

1.7 3D Molds and Whole Mounts

The extent of prostate cancer is usually underestimated at gross examination, due to the multifocal and heterogeneous characteristics of prostate cancer. The most effective method to prevent under-sampling is for the pathologist to sample the entire prostate. However, this is very time consuming and burdensome. Prostate specimens obtained after radical prostatectomy are usually processed as whole mount or as standard sections for pathological analysis. [12]

Whole mounts are 3D molds that are created by using magnetic resonance imaging (MRI) to map out the physical structure of the prostate. The prostate specimen are placed into the whole mounts. The mounts are equipped with slits spaced at a fixed interval to allow the laboratory technician to perform regulated cuts.

Whole mounts has the advantage over standard sections by showing the construction of the prostate by identifying and locating tumors in a more structured manner. Whole mounts creates

a reference to the index tumor and eases the comparison to preoperative diagnosing, such as MRI, digital rectal examination, trans-rectal ultrasound, and prostate biopsies. It allows the pathologist an improved overview of the prostate and improved identification of multiple tumor foci. In addition, it is much less time-consuming to cut and segment the prostate using whole-mounts. [12]

In this study, prostate cases equipped with whole mounts will feature up to 8 measurement points, while standard sections will feature up to 6 measurement points.

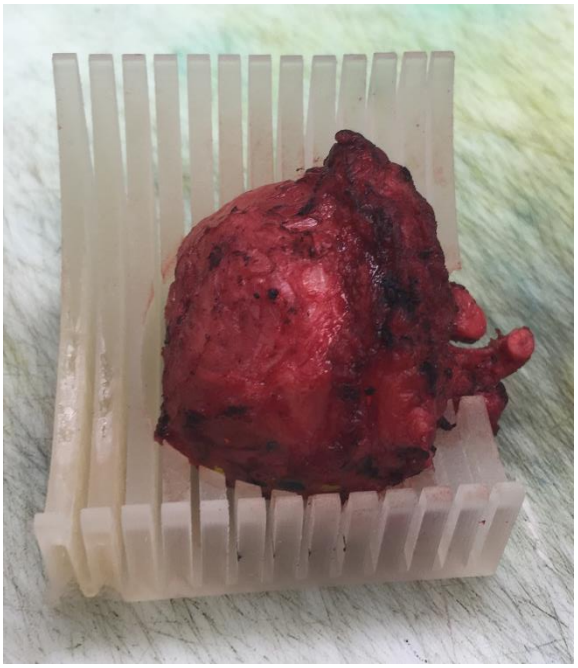

Figure 4: An image taken in the pathology lab of a prostate case placed into the 3D mold whole mount. The measurements were taken along the slits on both left and right lateral sides of the prostate.

1.8 Light Reflectance Spectroscopy

Light Reflectance Spectroscopy (LRS) is a noninvasive imaging modality that utilizes light scattering phenomena. LRS is used to measure the degree of light scattering and light absorption that result from varying chromophores at the cellular level. Light penetrates the tissue and undergoes random scattering events among the various chromophores and back scatters to escape the tissue in order to provide detection of diagnosis properties. [9]

The primary optical parameters of LRS include the reduced scattering coefficient, μ'_s, the absorption coefficient, μ_a, and the anisotropy factor, g. The reduced scattering coefficient, μ'_s, describes the scattering behavior of the photons in respect to the wavelength. It is a function of wavelength, λ. [9] The reduced scattering coefficient, $\mu'_s(\lambda)$, can be fitted using the following equations:

$$\mu'_s = \mu_s * (1 - g) \quad (1)$$

$$u_s = a\lambda^{-b} \quad (2)$$

Where μ'_s is the reduced scattering coefficient, μ_s is the effective scattering coefficient, g is the anisotropy factor, λ is the wavelength, "a" represents the scaling factor and scatter size, and "b" represents the scattering power. [10]

The absorption coefficient, μ_a (cm^{-1}), is the fraction of incident light that is absorbed by a light-absorbing medium and is dependent on the incremental path length the light travels throughout the medium. [9] The absorption coefficient μ_a can be calculated by the sum of all absorbing chromophore contributions, which primarily includes oxygenated hemoglobin [HbO], deoxygenated hemoglobin [Hb], and water concentration [$\%H_2O$]. These can be shown in equation 3.

$$u_a(\lambda) = [HbO]\varepsilon_{HbO}(\lambda) + [Hb]\varepsilon_{Hb}(\lambda) + [\%H_2O]\varepsilon_{H_2O}(\lambda) \qquad (3)$$

Where [HbO], [Hb], and [$\%H_2O$] represents the concentration of absorbing chromophores oxygenated hemoglobin, deoxygenated hemoglobin, and water concentration, respectively. And the extinction coefficient, represented by ε_{HbO}, ε_{Hb}, and ε_{H2O}, are multiplied to their corresponding chromophore concentration. [11] Other chromophores may be considered as well, such as melanin, fat, bilirubin, or beta-carotene. [9]

The reduced scattering coefficient and absorption coefficient together describe the diffusion of the photons in the tissue media, in regards to the random scattering light events in tissue. [9]

The anisotropy factor, g, describes the relative forward and backward direction of the scattered light. It is found by the equation, g = <cos Θ>, where Θ represents the angle deflection that results from the scattered photon. Multiple scattering events occur and the average Θ is calculated, and this is used to find the average value for the anisotropy factor, g. A high value of

g is representative of forward light penetration, but decreased backscattered light. Alternatively, a low value of g is representative of highly backscattered light, but less forward light penetration. [9]

The scattering events that occur in tissue most closely represents Mie scattering. Mie scattering is the scattering of both small and large sized spheres which is greater or equal to the wavelength of light. [9]

1.9 Photon Migration and Backscattering

As the optical probe is incident onto the capsule of the prostate tissue, the light is exponentially attenuated as the light propagates through the tissue. However, the photons are also backscattered at the early depths of penetration through the tissue. [13] As the photons encounter the scattering-inducing chromophores, the photons will change direction. The degree of the backscattered and reflected photons are dependent on the chromophores of the tissue. The density and cell nuclei size are factors that affect the scattering of the light. With more scattering-inducing elements, the photon will change direction many times at varying angles, eventually some photons will change direction into the opposite direction and backscatter towards the tissue exit. When the photons exit and return to the surface of the capsule of the prostate tissue. These backscattered photons are then detected by the optical probe and processed computationally to detect reflected scattering intensity.

The light scattering events are a probabilistic process, in which varying degree of scattering and absorption events will occur based on the scattering and absorbing properties of the different types of chromophores present in the tissue. Photons are assumed to be bundled as “packets”

or “bunches” of light and assumed to have a fixed initial weight. [13] This weight is reduced gradually due to attenuation or absorption events as the photon “packets” penetrates further into the prostate tissue.

Based off the Monios and Dimou model [13], a reflectance equation was developed to describe the behavior of the optical reflectance, Rp, of photons using short distance optical probe:

$$R_p = \frac{1}{k_1 \frac{1}{\mu_s'} + k_2 \frac{\mu_a}{\mu_s'}} \qquad (4)$$

Where, k1 and k2 are constant parameters that are dependent on various properties, such as the optical probe geometry, refractive index of the tissue, and the surrounding medium. These constant parameters can be determined experimentally. [14] And μ_s' is the reduced scattering coefficient and the μ_a is the absorption coefficient.

1.10 Light Reflectance Spectroscopy Prostate Cancer Applications

Light scattering intensity is highly dependent on the morphology of the tissue and is effective in differentiating between malignant and benign prostate tissue depending on the resulting spectral signatures. This modality is applied to detecting the positive surgical margins of prostate cancer. The surgeon will be able to utilize LRS in real-time during surgery by placing the LRS probe on a suspicious superficial location on the prostate capsule and determining with a certain degree of certainty if there is a positive surgical margin at that location. This information will help the

surgeon in a decision to remove excess surrounding tissue that corresponds to the measured location of the prostate capsule.

Chapter 2: Methodology

2.1 LRS Setup and Equipment

The apparatus of LRS for the detection of positive surgical margins for prostate cancer involves the use of an optical probe with a dimension of 1 mm in cross-sectional diameter with two inner 200 µm fibers for the source and detector. The source-detector separation distance is 370 µm. The source fiber is connected to a tungsten-halogen light source (HL2000HP, Ocean Optics, Inc., Dunedin, FL, USA), and the detector fiber is connected to a spectrometer (USB 2000+, Ocean Optics, Dunedin, FL USA) with a spectral range of 350 ~ 1200nm and analyzed using a Windows XP computer desktop. SpectraSuite (Ocean Optics, Inc., Dunedin, FL, USA) software is used to measure the optical properties and optical intensity from the detected light, producing a spectral signature along a broadband of wavelength values, typically from ~465nm to ~1140nm.

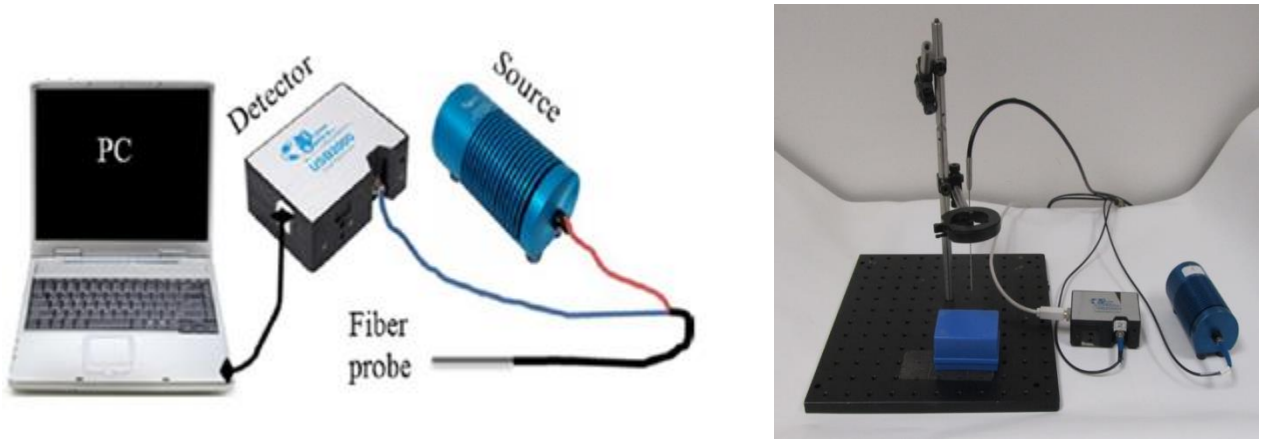

Figure 6: The typical setup for an LRS system. This includes a broadband light source that emits light into the optical probe and onto the scattering media. The light backscatters and reflects off the scattering media and returns to the optical probe and is detected by the spectrometer. The spectrometer divides the light into its individual wavelengths and outputs the data into the computer. [15]

2.2 LRS Measurement Methodology

The measurements are performed at the University of Texas Southwestern (UTSW) Medical Center, Dallas, TX. Fresh *ex vivo* prostate specimens are immediately obtained from patients undergoing laparoscopic radical prostatectomy or robotic-assisted laparoscopic radical prostatectomy. [1,2] The specimen is received in the pathology laboratory for measurements.

The fresh *ex vivo* prostate specimen may either be processed as whole mount or standard sections case. Regardless of the case, the prostate specimen is first examined by tactile contact on the left and right lateral sides of the prostate. The surgeon is most concern with the left and right lateral sides of the prostate because positive surgical margins of the tumors are prone to develop in those regions. Any dense or nodular structures that are felt under the capsule of the prostate are noted. These regions are suspicious for tumors and will be subjected to LRS measurements.

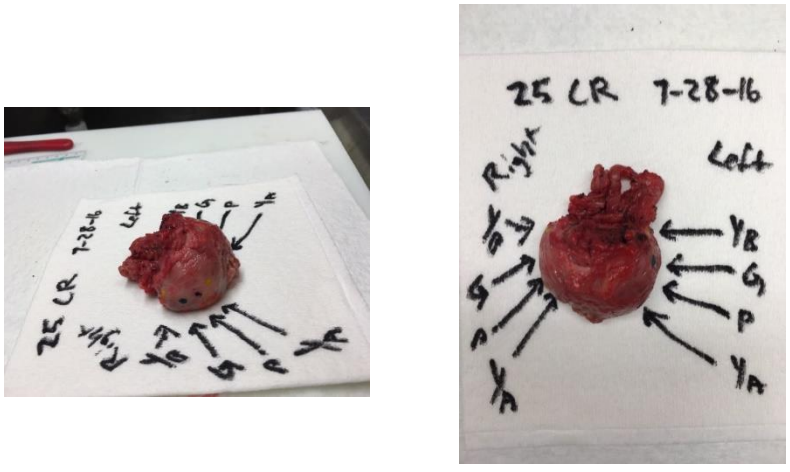

Figure 7: A top and side view of a prostate specimen revealing how and where typical ink marks are made. Generally 3 or 4 ink markings of red, yellow, green, or purple are made to identify LRS measurement locations on the left and right lateral sides of the prostate.

If the prostate specimen case is a standard section case, typically three LRS measurements will be performed at the base, middle, and apex regions on the left lateral side and three measurements are made on the corresponding right lateral sides. The three measurement locations on the left and right lateral sides are roughly aligned along the same transverse planes.

In the whole mount case, there are four measurements that are made on the left lateral side and four measurements made on the right lateral side, for a total of eight measurements. The whole mount mold have "slits" that are spaced at a regular intervals of ~4mm, and thus more accurate transverse correlations can be made from the left and right lateral sides. This allows more room to perform an additional measurement on each lateral side of the prostate. The prostate is placed and properly oriented into the whole mount and four transverse planes are chosen along the left and right lateral sides for LRS measurements.

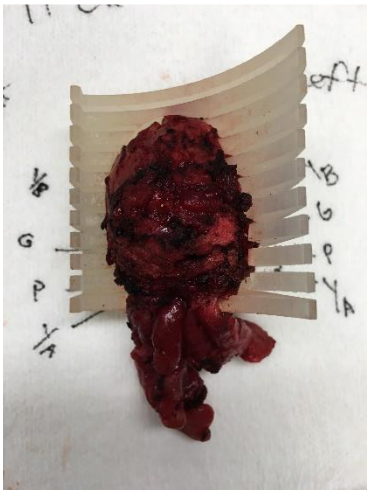

Figure 8: An image of a prostate case placed in a whole mount. The slits help with selecting locations for LRS measurements on the same transverse plane on both left and right lateral regions of the prostate. Typically a total of 8 LRS measurements are performed on whole mount cases.

After selecting the regions of the left and right lateral side to be measured, the prostate is then placed securely on the LRS stage. The needle probe is then incident normal to the surface of the margin of the prostate and measures a point on the selected region. The procedure here is the same regardless if it is a standard section or whole mount case.

The LRS apparatus then measures the intensity of the reflected photons and outputs the results onto the Windows XP computer using SpectraSuite. The integration time is set to 27 ms and the dark noise is removed before recording the measurements. After recording a LRS measurement point, the measured point is inked with either the colors yellow, green, purple, or red. The colors serve as identification points for the pathologists to perform her analysis for positive surgical margins of cancer or normal prostate tissue. The pathologist reports a '0' for no cancer tissue, '1' for positive margin of cancer, or '2' for near positive margin of cancer. These measurements are repeated for the remaining measurement points, for up to six measurement points on standard section cases and up to eight on whole mount cases.

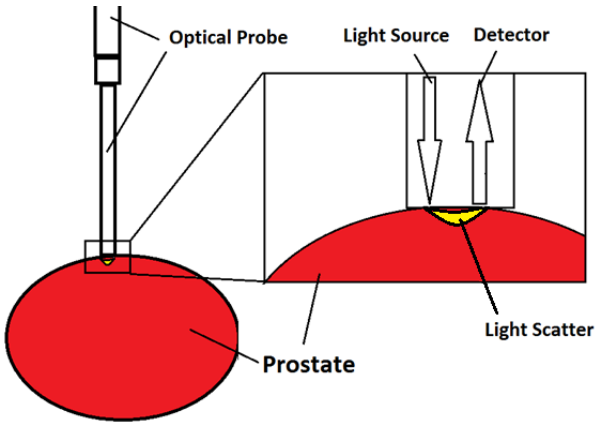

Figure 9: A schematic showing how reflected and backscattered light interacts when the optical probe is incident normal to the surface of the prostate tissue. The reflected light forms a "banana shape" pattern within the prostate tissue.

2.3 Cancer Classification Algorithm and the 5 and 9 Feature Selection using MATLAB

The spectral signature data, obtained from SpectraSuite, of each LRS measurement are first processed by dividing the raw data by a reference "white" sample. This is done in order to calibrate and filter the spectral signature data and to normalize the data to obtain the pure spectral signal. This filtered spectral signature data is then processed using algorithms in MATLAB that extracts certain features. The features extracted are dependent on two algorithms that are used for prostate cancer classification: The 5 Feature Algorithm and the 9 Feature Algorithm.

The 5 Feature Algorithm was developed by Dr. Zeng Li, PhD., and a previous graduate student Mr. Xinlong Wang, PhD candidate. [15] Specific features were selected and then extracted from the 50 prostate cases collected by Xinlong during his previous work on this research. In total, there were 187 measurement points, 32 of which were pathologically confirmed as cancer and 155 of which were pathologically confirmed as normal prostate tissue. The features of the 187 measurement points were cross referenced with the pathology results, correlating the feature data with '1' for cancerous measurement points and correlating the feature data with a '0' for normal tissue measurement points. This data set served as the "training data" set that will be used to classify the "testing data" set. In MATLAB, the Generalized Linear Model function is used to help learn and distinguish specific combinations of feature patterns that are associated with cancerous readings from specific feature patterns that are associated with normal tissue readings, based off the training data set from Xinlong's data. This is applied onto the data Henry has collected, the "testing data", and the algorithms performs a decision for cancer classification

and outputs a ‘1’ for cancerous readings and outputs a ‘0’ for normal reading. This process is displayed in the flowchart shown in Figure 10.

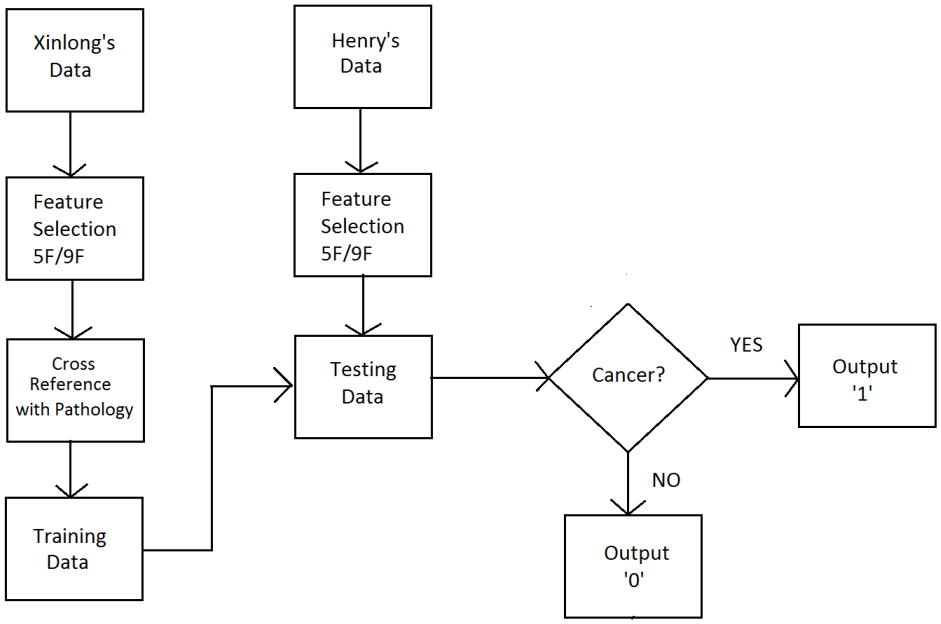

Figure 10: A flowchart that outlines the cancer classification algorithm using the raw data obtained from Xinlong’s data and extracting specific features. The features are cross referenced with the pathology results to associate specific feature combinations to cancer or normal prostate readings. This forms the training data set. The same features are also extracted from the raw data that is collected by Henry. This data forms the testing data set. A generalized linear model is applied, using MATLAB, to associate specific feature patterns to cancer readings and associate specific feature patterns to normal readings, based off the training data set. This model is applied to the testing data set in order to create a cancer classification decision, outputting a ‘1’ for cancer readings or a ‘0’ for normal readings.

The algorithm is highly dependent on the feature selections from the raw data. In Xinlong’s work, he isolated 5 features from the spectral signature, in which he termed a’, b’, c’, d’, and e’. The features a’ and b’ represent the slope and intercept of the spectral signature from the 630 nm to 830 nm range. The feature c’ represents the slope from 580 n m to 600 nm, feature d’ represents

the difference between the peak at 610 nm to 640 nm and the “W” shape at 527 nm to 582 nm, and feature e’ represents the height at 750nm.

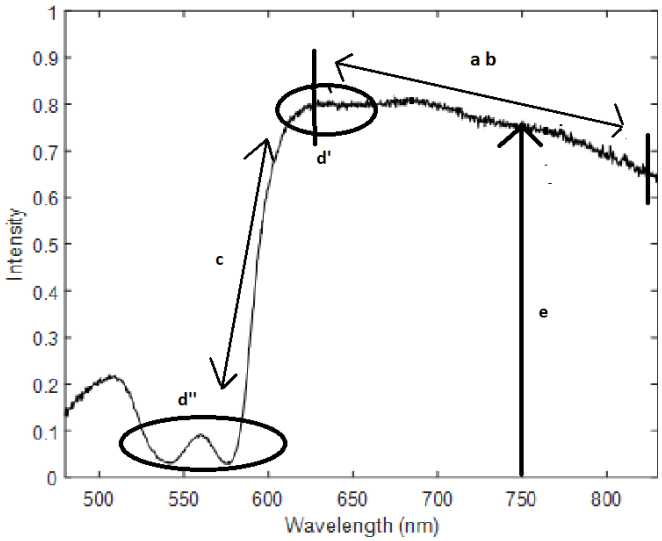

Figure 11: The 5 Feature Algorithm; a: Slope at 630 – 830nm, b: Y-Intercept at 630 – 830nm, c: Slope at 580 – 600nm, d: Peak average (610 – 640nm) minus W shape average (527 – 582nm), and e: Height at 750nm.

In the 9 Feature algorithm, additional features were selected. Features c’, d’, and e’ were kept but the slope and intercept from the ~600nm to ~860nm range were divided into three separate slopes and intercepts due to a consistent trend of change in slopes at 690 nm and at 770 nm. Features a1’, b1’, a2’, b2’, a3’, and a4’ were introduced where a1’, a2’, and a3’ represent the slopes from 630 nm to 690 nm, 690 nm to 770 nm, and 770 nm to 830 nm, respectively. And b1’, b2’, and b3’ represents the y-intercepts from 630 nm to 690 nm, 690 nm to 770 nm, and 770 nm to 830 nm, respectively.

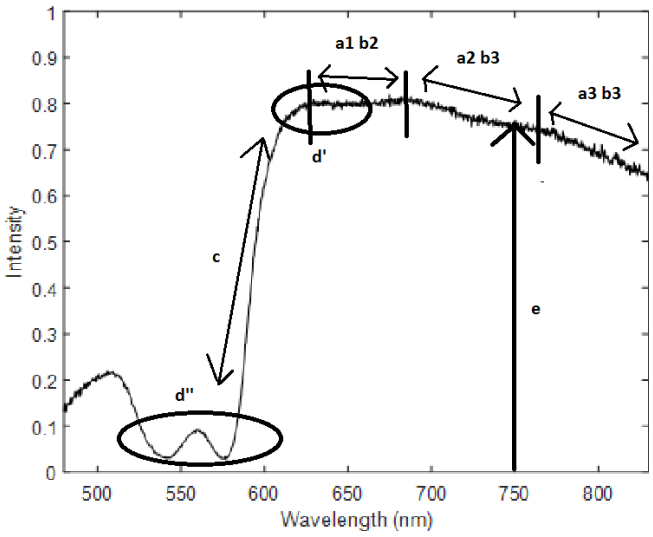

Figure 12: The 9 Feature Algorithm; a1 and b1: Slope and Intercept at 630 – 690nm, a2 and b2: Slope and Intercept at 690 – 770nm, a3 and b3: Slope and Intercept at 770- 830nm, c: Slope at 580 – 600nm, d: Peak average (610 – 640nm) minus W shape average (527 – 582nm), and e: Height at 750nm.

This decision output from the algorithm is then compared to the true pathology results for Henry's data. And the Sensitivity (Sen), Specificity (Spc), Positive Predictive Value (PPV), Negative Predictive Value (NPV), and Accuracy (Acc) can be calculated. The data is further divided based on the Gleason Group with the aid of Dr. Igor Sorokin, MD. The measurement data was divided into Gleason Group 1 (Gleason Score 6), Gleason Group 2 (Gleason Score 3+4), Gleason Group 3 (Gleason Score 4+3), and Gleason Group 4 (Gleason Score 4+4).

2.4 Pressure Analysis

When applying the optical probe normal to the surface of the prostate capsule for measurements, there is a concern if the pressure applied by the optical probe will affect the spectral reading of the LRS system. This study employs the use of a scale, with a resolution in milligrams, and the use of the LRS system mentioned in Section 2.1.

(a) (b) (c)

Figure 13: In the photos, (a) represents the scale with a resolution of milligrams. Photo (b) represents the measurement of the axial displacement of the optical probe using a ruler. The optical probe is translated axially per millimeter onto the surface of the prostate. Photo (c) shows how the optical probe makes contact with surface of the prostate. The optical probe is translated at a distance of -1 mm (1 mm above the surface), 0 mm (at the surface), 1 mm, 2 mm, 3 mm, and 4 mm of axial displacement onto the surface of the prostate.

The pressure analysis was performed on a total of three prostate specimens, with six readings per prostate at different location sites on the prostate. Generally the measurements were

performed at the base, mid and apex region on both the left and right lateral locations on the prostate surface. At each measurement location, there are six total LRS measurements at -1 mm (1 mm above the surface of the capsule), 0 mm (at the surface of the capsule), 1 mm, 2 mm, 3 mm, and 4 mm of axial displacement onto the surface of the prostate capsule. Thus there are a total of 18 different measurements per axial displacement of the probe.

2.5 Penetration Depth of the New Optical Probes

Two new optical probes were designed and ordered from Ocean Optics, Inc. The first optical probe, termed "New 370 µm", was designed to replace the "Old 370 µm" probe. And the second optical probe, termed "125 µm", was designed to detect more superficial tumors to the outer capsule of the prostate.

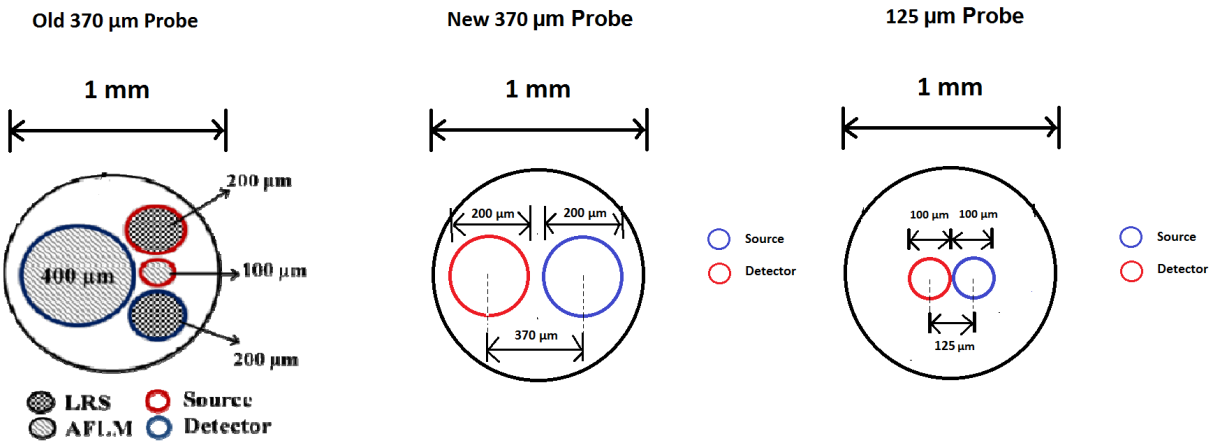

(a) (b) (c)

Figure 14: (a) The Old 370 µm optical probe with a separation distance of 370 µm from center to center of source and detector, (b) the New 370 µm optical probe with a separation distance of 370 µm from center to center of source and detector, and (c) the 125 µm optical probe with a separation distance of 125 µm from center to center of source and detector.

The “Old 370 µm” probe was originally designed with four fibers for the use of LRS and Auto-Fluorescence Lifetime Spectroscopy (AFLM). In the current study, the AFLM fibers are no longer used. The LRS fibers involve two fibers, the source and detector fibers, each with a 200 µm diameter. The separation distance between the two fibers is approximately 370 µm from center to center of the fibers. The cross-sectional diameter of the actual probe is 1 mm. The “New 370 µm” was designed to mimic the dimensions of the “Old 370 µm”, while excluding the AFLM fibers. The “New 370 µm” probe also has a cross-sectional diameter of 1mm and also has two 200 µm fibers (source and detector) with a separation distance of approximately 370 µm from center to center. The “125 µm” fiber was designed to have a similar probe dimension of 1 mm in cross-sectional diameter, but has two fibers (source and detector) with a diameter of 100 µm. The separation distance from the source fiber to the detector fiber is approximately 125 µm from center to center.

The experiment to track the penetration depths of the three optical probes involved the use of Intralipid fluid, a fat emulsion solution. This solution is an ideal scattering media to measure the backscattering of the light emitted by the probes due to the high lipid content. Lipids are chromophores with high scattering properties. The scattering properties of prostate tissue are closely related to an Intralipid solution of 1%, thus the Intralipid solution was created at 0.8% and 1.2%. The solution was created by mixing 40 mL of 20% Intralipid solution with 960 mL of water to form a 0.8% concentration of Intralipid solution. And the second solution was created by mixing 60 mL of 20% Intralipid solution with 940 mL of water to form 1.2% concentration of Intralipid solution.

Either solution, 0.8% or 1.2%, was filled into a container as seen in (a) from Figure 15. The container holds a cup that is equipped with a black absorbing slope as seen in (c) from Figure 15, which will serve to measure the penetration depth of the light from the optical probes. Essentially the container will be translated to the left, as the optical probe remains in a fixed space. The end of the optical probe is submerged below the surface of the Intralipid solution to prevent light leakage and to effectively measure the reflected light.

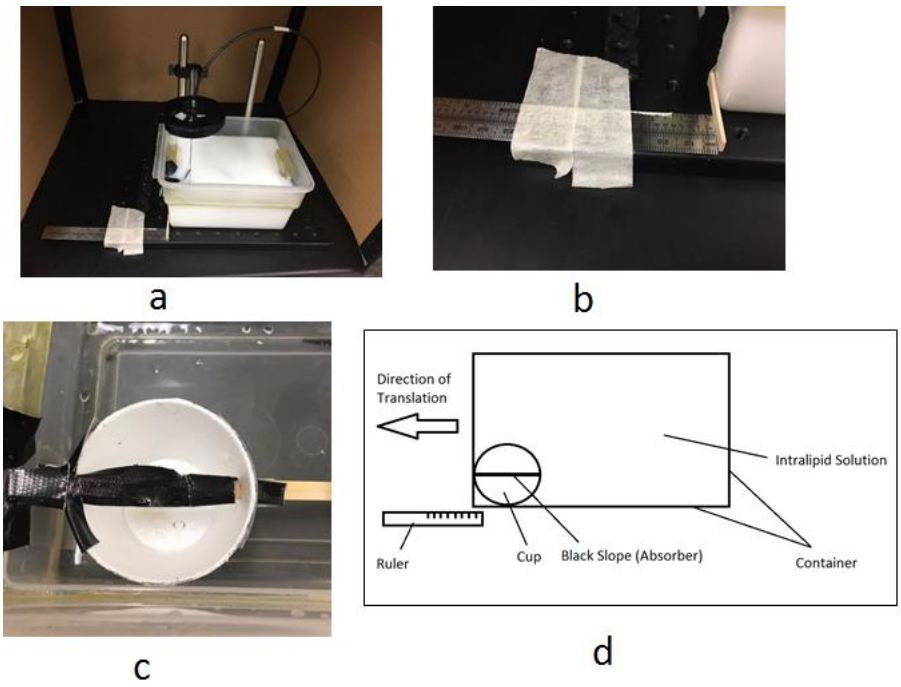

Figure 15: (a) The system setup with the container equipped with the cup and absorber. The container is filled with Intralipid solution of either 0.8% or 1.2%. The optical probe is fixed above the system and submerged under the solution. (b) A ruler that measures the lateral translation of the system. (c) The cup equipped with a black absorbing slope. (d) A schematic of the system, showing the container, cup, black slope, and ruler. The system is being translated to the left.

As the container is translated to the left in millimeter increments, the optical probe will emit light onto the black absorbing slope. At the initial translation distance of C = 0 mm, the optical probe makes physical contact with the peak of the black absorbing slope, where the majority of the light will be absorbed. As the system is translated to the left, per millimeter increments, less light will be absorbed by the black slope and an increasing amount of light will be reflected and detected by the optical probe in a saturation curve pattern.

The penetration depth can be calculated based off the Similar Triangle Rules, as seen in Figure 16. The ratio of the opposite and adjacent sides of the larger triangle is equal to the ratio of the opposite and adjacent sides of the smaller triangle, where A/B = D/C. 'A' represents the length of the opposite side of the larger triangle at 11 mm, and 'B' represents the length of the adjacent side of the larger triangle at 62 mm. 'C' represents adjacent side of the smaller triangle and is the translational distance (mm) of the system and serves as the independent variable. The penetration depth 'D' represents the opposite side of the smaller triangle and can be calculated based on these values, where D = 0.17742 * C.

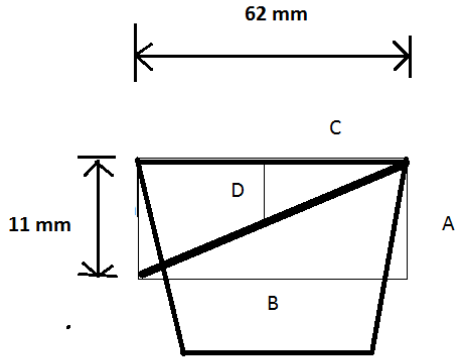

A/B = D/C

C = Translation Distance
D = Penetration Depth

D = (A*C)/B

D = 0.17742 * C

Translation (mm)	Penetration Depth (mm)
0	0
1	0.17742
2	0.35484
3	0.53226
4	0.70968
5	0.8871
6	1.06452
7	1.24194
8	1.41936
9	1.59678
10	1.7742
11	1.95162
12	2.12904
13	2.30646
14	2.48388
15	2.6613
16	2.83872
17	3.01614
18	3.19356
19	3.37098
20	3.5484

Figure 16: The image on the left shows a cup that holds a black absorbing slope. Based on the similar triangle rule, the penetration depth can be calculated. The ratio of the opposite and adjacent sides of the larger triangle is equal to the ratio of the opposite and adjacent sides of the smaller triangle. The length of the opposite side 'B' of the larger triangle is 11 mm and the length of the adjacent side 'A' of the larger triangle is 62 mm. The translation distance 'C' is the independent variable applied and the penetration depth 'D' is the dependent variable to be calculated via the equation: D = 0.17742*C. A table on the right is shown to show how the translation distance 'C' correlates with the penetration depth 'D'.

2.6 New 2 and 4 Feature Methodology

A new algorithm was develop that emphasized the wavelength ranges from ~610 nm to ~ 900 nm in an effort to apply emphasis on the wavelength range that were significant based on a statistical two sample t-test. This range completely eliminates the spectral signal caused by blood, in terms of hemoglobin and deoxyhemoglobin concentrations. In addition, selecting two or three wavelengths may prove beneficial for the potential development of a new LRS system using Light-emitting Diodes (LED) and greatly reducing costs of the LRS system, which is ideal for commercialization. Each LED will emit a specific wavelength and employing two or three wavelengths are all that is necessary in order to calculate the slope and y-intercept between these wavelength values.

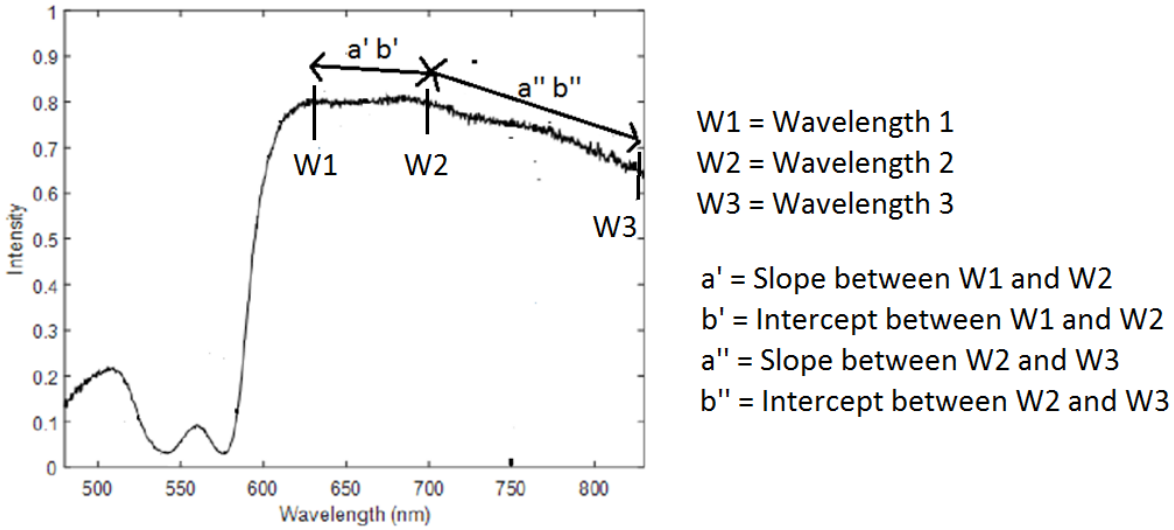

Figure 17: The 2/4 Feature Algorithm; a' and b': Slope and Intercept between Wavelength 1 (W1) and Wavelength 2 (W2); a'' and b'': Slope and Intercept between W2 and Wavelength 3 (W3).

The 2 and 4 Feature Algorithm operates similarly to the algorithm in Section 2.3. The difference is in the feature selection. In the 2 Feature Algorithm, two wavelengths, W1 and W2, are selected within the ~600 nm - ~900 nm range. And the slope, a', and y-intercept, b', can be calculated from these two points. The 4 Feature Algorithm also selects wavelengths within the ~600 nm - ~900 nm range. In the 4 Feature Algorithm, three wavelengths, W1, W2, and W3, are selected and the slope and y-intercept, a' and b', are found between W1 and W2, and the slope and y-intercept, a'' and b'', are found between W2 and W3. The values for W1, W2, and W3 can be tuned for optimal cancer classification.

Chapter 3: Results

3.1 Demographics of Patients in Henry's Study

In total, there were 47 patients who were enrolled into this study. The average age of the patient groups was 61.7 years, and the patient groups were further divided into their corresponding Gleason Score (GS). The prostate specimens were obtained from each patient via radical robotic assisted prostatectomy. The Gleason Score group were organized into Group 1 (GS 6), Group 2 (GS 3+4), Group 3 (4+3), and Group 4 (GS 4+4). Group 1 consisted of 4 specimens, Group 2 consisted of 32 specimens, Group 3 consisted of 4 specimens, and Group 4 consisted of 7 specimens. Based off the general demographics of the prostate specimens, Group 2 has a much higher number of specimens than Groups 1, 3, and 4. This implies that the overall dataset will be highly biased towards Group 2.

Gleason Group	**Number of Prostate Specimens**
Group 1 (GS 6)	4
Group 2 (GS 3+4)	32
Group 3 (GS 4+3)	4
Group 4 (GS 4+4)	7
Total Number of Patients	47

Figure 18: Demographics of the prostate specimens, divided into Gleason Group 1, Group 2, Group 3, and Group 4.

3.2 Filtered Tissue Data

After performing the LRS measurements in the pathology lab, the measurement spots on the prostate specimens were inked with either yellow, green, red, or purple ink. However, during the logistical processing of the prostate specimen, a number of ink markings faded or were unidentifiable by the pathologist. The left lateral side of the prostate is generally coated in blue ink to act as a regional identifier for the pathologist. Often times the purple ink LRS measurements would blend with the blue ink background and made it very difficult for the pathologist to distinguish between the two ink colors.

In addition, in an effort to reduce the "noise" associated with irregular tissue data, a number of LRS measurements were also removed based off detailed notes of LRS measurements. "Irregular tissue" is defined as a LRS measurements performed on sites with adhesion or connective tissue, neuromuscular tissue, fatty tissue, or near suture sites. These different tissue types and chromophores may possess varying spectral properties that can affect the LRS spectral readings. In this study, the emphasis is on the LRS measurements performed on smooth surfaces of the prostate capsule and to detect the presence of cancer that is near or at the margin of the prostate capsule.

3.3 Demographics of Prostate Measurements in Henry's Study

There were a total of 358 LRS prostate measurements performed over the course of the study. After removing a number of LRS prostate measurements, based off the filtered tissue data from Section 3.2, there were 257 total measurements after filtering. Group 1 (GS 6) had a total of 24 LRS prostate measurements, Group 2 (GS 3+4) had a total of 173 LRS prostate measurements,

Group 3 (GS 4+3) had a total of 22 LRS prostate measurements, and Group 4 (GS 4+4) had a total of 38 LRS prostate measurements. Based off this data, Group 2 has a significantly higher number of LRS prostate measurements than Groups 1, 3, and 4. This implies that the overall data set is highly biased towards Group 2 with a GS of 3+4.

Gleason Group	**Number of LRS Prostate Measurements**
Group 1 (GS 6)	24
Group 2 (GS 3+4)	173
Group 3 (GS 4+3)	22
Group 4 (GS 4+4)	38
Total Number of LRS Prostate Measurements	257

Figure 19: Demographics of the LRS prostate measurements, divided into Gleason Group 1, Group 2, Group 3, and Group 4.

3.4 Cancer vs Normal Tissue LRS Measurement Readings

The average cancer tissue readings were compared to the average normal prostate tissue readings. The cancer tissue and normal prostate tissue readings were based off the pathology report, which represents the true value at each LRS prostate measurement point. The pathology report provides a value of either '0', '1', or '2' for each LRS measurement point. A '0' represents normal prostate tissue and no cancerous tumors near the site of the LRS measurement point. A '1' represents cancerous tissue at the margin of the LRS measurement point. This is termed as a "positive surgical margin", in which the cancerous tissue has invaded through the prostate capsule and potentially to the surrounding tissue around the prostate. A '2' represents a LRS

measurement point where there is cancerous tissue near the margin of the prostate capsule, but not beyond or at the margin of the prostate capsule. The depth of the cancerous tissue from the outer capsule of the prostate is also reported in millimeters for values of '2'.

LRS prostate measurements with a reported '1' or '2' were grouped into the cancer tissue readings and measurements with a reported '0' were grouped into the normal prostate tissue readings. The average and the standard deviations of the cancer readings were found and compared to the average and standard deviations of the normal prostate readings.

In the first graph (A) of Figure 20, it compares the total number of measurement points of 358 readings where the sample size for cancer tissue was 59 and the sample size of the normal prostate tissue was 299. After filtering the irregular tissue data, the total number of measurement points was reduced to 257, where the sample size of the cancer tissue was reduced to 54 and the sample size of the normal tissue was reduced to 203. This can be seen in Figure 20 (B).

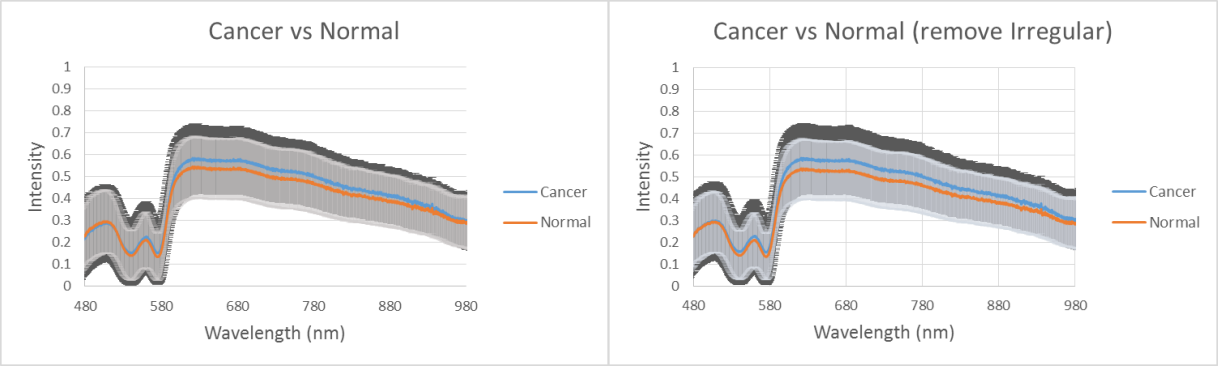

(A) (B)

Figure 20: (A) Graphic comparison of the average cancer tissue (n = 59) spectral curve vs the average normal prostate tissue (n = 299) spectral curve. This graph includes all irregular tissue data mentioned in Section 3.2. (B) Graphic comparison of the average cancer tissue (n = 54) spectral curve vs the average normal prostate tissue (n = 203) spectral curve. This graph excludes all irregular tissue data mentioned in Section 3.2.

3.5 Comparison of Cancer vs Normal Tissue Data Based off the Gleason Score

The average spectral curves of the normal prostate tissue data was compared against the average cancer tissue data, and the average cancer tissue data was further divided based off the Gleason Score. The Gleason Score was divided into GS 6, 3+4, 4+3, and 4+4. As expected, the average normal tissue has the lowest intensity at the peak intensity at approximately 0.53 at 620 nm. Gleason Score 6 and 3+4 have very similar intensity values, both having a peak intensity at approximately 0.57 at 620nm. Gleason Score of 4+3 has an obvious increase in the peak intensity at approximately 0.63 compared to the previous three groups at 620 nm. And Gleason Score of 4+4, as expected, has the highest peak intensity value of 0.67 at 620 nm wavelength. This data implies that GS of 6 and 3+4 measurement locations were potentially performed primarily on

Gleason Grade of 3, which outputted low peak intensity values. And GS of 4+3 and 4+4 were performed primarily on the Grade 4 measurement locations which are consistent with higher intensity values. This can be seen graphically in Figure 21.

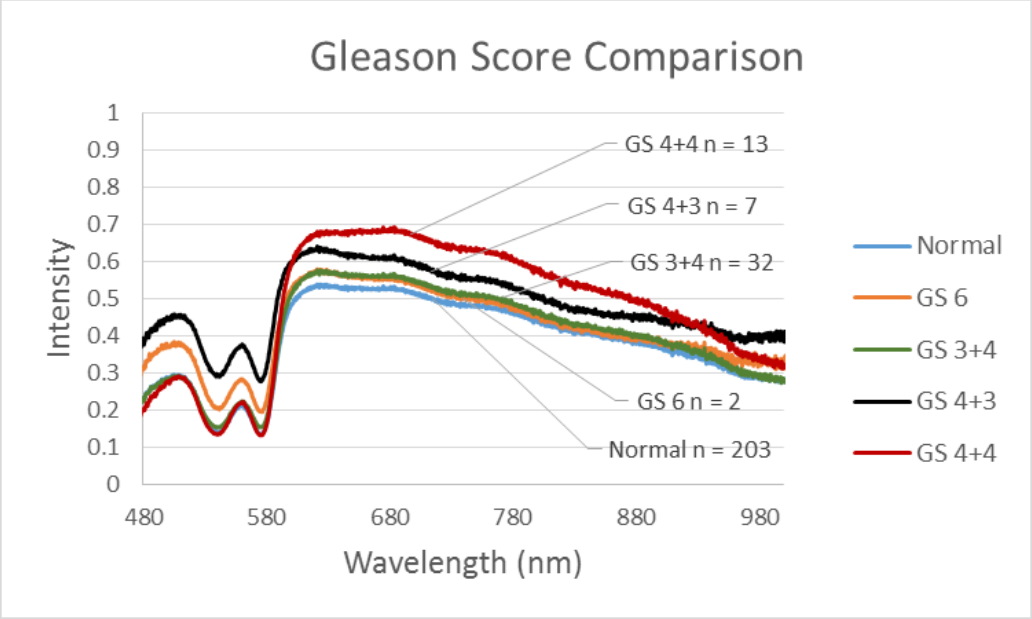

Figure 21: This graph summarizes the average spectral intensity curves associated with normal prostate tissue (n = 203), cancer tissue with GS 6 (n = 2), cancer tissue with GS 3+4 (n = 32), cancer tissue with GS 4+3 (n = 7), and cancer tissue with GS 4+4 (n = 13).

The average spectral curves were compared and analyzed with the standard deviation between the average normal groups (n = 203) versus the average cancer groups of GS 6, 3+4, 4+3, and 4+4. In Figure 22, the first graph (A) compares the average spectral curve of normal prostate tissue to the average spectral curve of cancer with a GS of 6 (n = 2). The average GS 6 curve is only slightly higher than the average normal prostate tissue curve, but the standard deviations from both groups overlapped considerably. This implies that differentiating between the two spectral

groups will be difficult. In the second graph (B), it compares the average spectral curve of normal prostate tissue to the average spectral curve of cancer with a GS of 3+4 (n = 32). The average GS 3+4 curve was also only slightly higher than the average normal curve, and the standard deviations from both groups overlapped considerably as well. This implies that differentiating between normal prostate tissue and GS 3+4 would also prove to be difficult. In the third graph (C), it compares the average normal prostate tissue to the average cancer tissue with a GS of 4+3 (n = 7). For the GS 4+3 group, there is an obvious higher average intensity curve, compared to the average normal prostate tissue curve. However, there is still some degree of overlapping in the standard deviations between the two groups, but differentiating between the two groups will prove less of a challenge when compared to the GS 6 and GS 3+4 groups. In the fourth graph (D), it compares the average normal prostate tissue curve to the average cancer curve with a GS of 4+4 (n = 13). There is a significant difference between the GS 4+4 curve and the normal prostate tissue curve. The GS 4+4 group has the highest intensity compared to the GS 6, 3+4, and 4+3 groups, and it shows the greatest separation distance from the average normal prostate tissue curve. The standard deviation between the average GS 4+4 group and the average normal prostate tissue group show smaller degree of overlapping, which implies differentiating between these two groups would be considerably easier compared to the average GS groups of 6, 3+4, and 4+3.

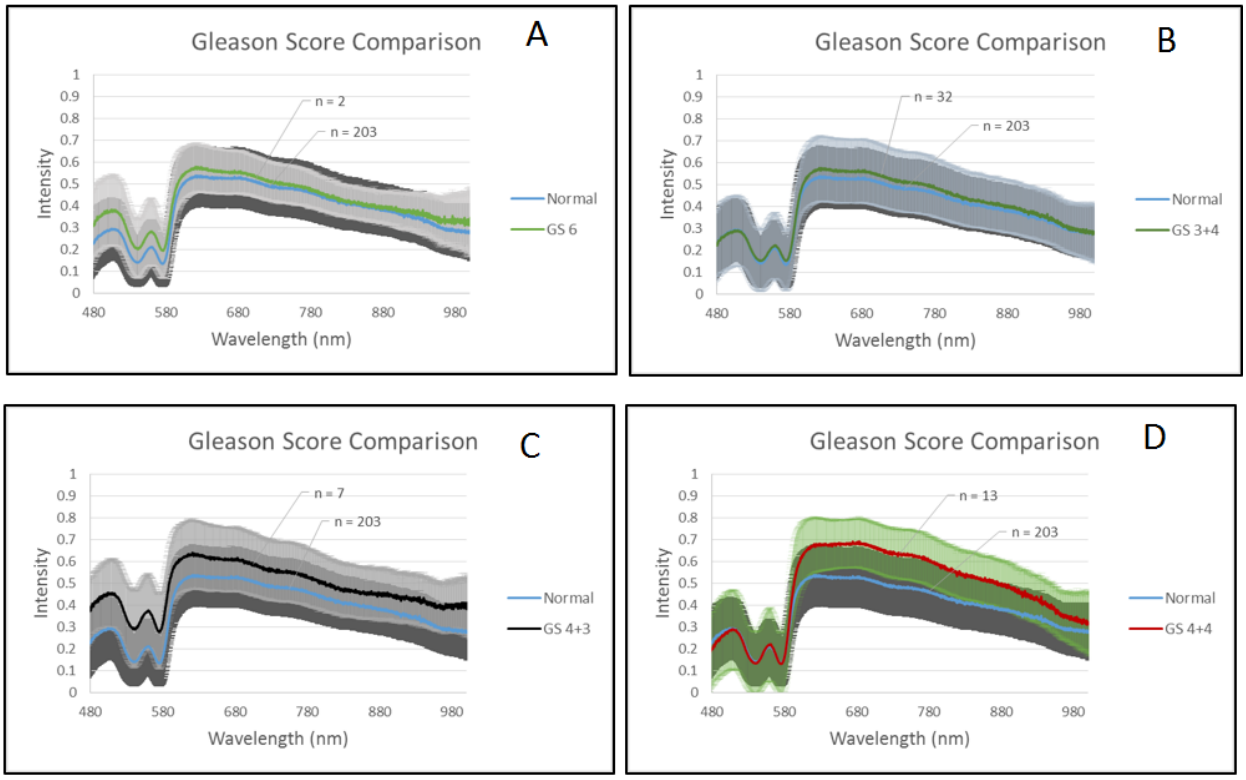

Figure 22: (A) A graphical comparison of the spectral curves between the average normal prostate tissue and the average cancer tissue with a GS of 6. (B) A graphical comparison of the spectral curves between the average normal prostate tissue and the average cancer tissue with a GS of 3+4. (C) A graphical comparison of the spectral curves between the average normal prostate tissue and the average cancer tissue with a GS of 4+3. (D) A graphical comparison of the spectral curves between the average normal prostate tissue and the average cancer tissue with a GS of 4+4.

3.6 Algorithm Comparison: 5 Feature and 9 Feature

The 5 Feature and the 9 Feature algorithms were both performed on the same set of collected test data from Henry's study. Both algorithms had the same training set from Xinlong's study. The two algorithms differed by the feature selection used for cancer classification using LRS. Refer to Section 2.3 for an in depth review of the methodology for the 5 Feature and 9 Feature Algorithms.

The resulting data from the 5 Feature and 9 Feature Algorithm were compared by first dividing the data based on the Gleason Groups, into Gleason Group 1 (GS 6), Gleason Group 2 (GS 3+4), Gleason Group 3 (4+3), and Gleason Group 4 (GS 4+4). The values for Sen, Spc, PPV, NPV, and area under the curve (AUC) were compared. The Sen is calculated by the equation Sen = TP/(TP + FN), where TP represents the True Positives (TP) and FN represents the False Negatives (FN). The Spc is calculated by the equation Spc = TN/(TN + FP), where TN represents the True Negatives (TN) and FP represents the False Positives (FP). The PPV is calculated by the equation PPV = TP/(TP + FP). The NPV is calculated by the equation NPV = TN/(TN + FN). [16, 17]

From Figure 23, in Gleason Group 3, the 5 Feature Algorithm was shown to be consistently greater than the 9 Feature Algorithm in all five categories of Sen, Spc, PPV, NPV, and AUC with values of 42.90%, 93.30%, 75.00%, 77.80%, and 68.10%, respectively. However, the 9 Feature Algorithm had the same value as the 5 Feature Algorithm with a value of 93.30%. In Gleason Group 4, the 5 Feature Algorithm had higher values in three categories of Sen, NPV, and AUC with values of 72.70%, 88.00%, and 77.10%, respectively, compared to the 9 Feature Algorithm. The 9 Feature Algorithm had greater values in the Spc and PPV category with values of 88.90% and 66.70%, respectively. Based on these data, we can conclude that the 5 Feature Algorithm is the optimal algorithm used for cancer classification.

Looking closely as the Sen for 5 Feature Algorithm for Gleason Groups 1, 2, 3, and 4, the values are 50.00%, 40.70%, 42.90%, and 72.70%, respectively. Based off previous research [14, 15], LRS was concluded to be ineffective for GS 6, which comprises of Gleason Grade 3. Gleason Groups 1, 2, and 3 all contains Gleason Grade 3, which implies the measurement may have been performed on a Gleason Grade 3 location. This would explain the low Sen values for these three

groups. In Gleason Group 4, the Gleason Grade is primarily a Gleason Grade 4. As a result, the Sen is much higher than the other three groups, at a value of 72.70%. This implies that LRS is significantly more effective for cancer grades of Gleason Grade 4 than Gleason Grade 3. In the future, pathology would need to report the Gleason Grade at the measurement location in order to accurately validate the data analysis.

	Gleason Group 1 (GS 6)		Gleason Group 2 (GS 3+4)		Gleason Group 3 (GS 4+3)		Gleason Group 4 (GS 4+4)	
	5 pt algorithm	9 pt algorithm	5 pt algorithm	9 pt algorithm	5 pt algorithm	9 pt algorithm	5 pt algorithm	9 pt algorithm
Sensitivity	50.00%	50.00%	40.70%	29.60%	**42.90%**	28.60%	**72.70%**	54.50%
Specificity	68.20%	81.80%	80.10%	88.40%	**93.30%**	**93.30%**	81.50%	**88.90%**
PPV	12.50%	20.00%	27.50%	32.00%	**75.00%**	66.70%	61.50%	**66.70%**
NPV	93.80%	94.70%	88.00%	87.20%	**77.80%**	73.70%	**88.00%**	82.80%
AUC	59.10%	65.90%	60.40%	59.00%	**68.10%**	61.00%	**77.10%**	71.70%

Figure 23: A comparison of the 5 Feature Algorithm with the 9 Feature Algorithm in terms of Sen, Spc, PPV, NPV, and AUC. The data is further divided into their respective Gleason Groups 1, 2, 3, and 4.

3.7 Pressure Analysis Results

There was a concern if applying an excessive amount of pressure would affect the spectral reading from the LRS system. The methodology of performing the pressure analysis are explained in Section 2.4.

The axial displacement of the probe, measured in millimeter increments, was compared to the pressure of the optical probe. The pressure of the optical probe was calculated by measuring the mass (g) of the prostate at each level of axial displacement (-1, 0, 1, 2, 3, 4 mm) and then multiplying the mass by the factor 0.0098, based off Vikrant's previous work in pressure analysis. [18] This results in the weight (N) at each level of axial displacement. The net increase in weight was found at each increment level of axial displacement applied. The pressure, measured in

N/mm^2, can be calculated by dividing the net weight (N) by the cross-sectional area of the optical probe of 1 mm^2.

In Figure 24 (A) below, as the axial displacement of the probe is increased, the average pressure increases in an exponential fashion. In addition, as the axial displacement becomes higher, particularly at 4 mm, the standard deviation varies substantially. This graph can be cross validated with the graph in Figure 24 (B), which compares the correlation between the axial displacement of the probe to the average reflected light intensity, measured using the LRS system at 630 nm wavelength. The average intensity analysis graph reveals that as the axial displacement of the probe is increased, the average intensity of the reflected light does not vary considerably, and remains at the intensity of approximately ~0.5 from 0 mm (surface of prostate) to 4 mm.

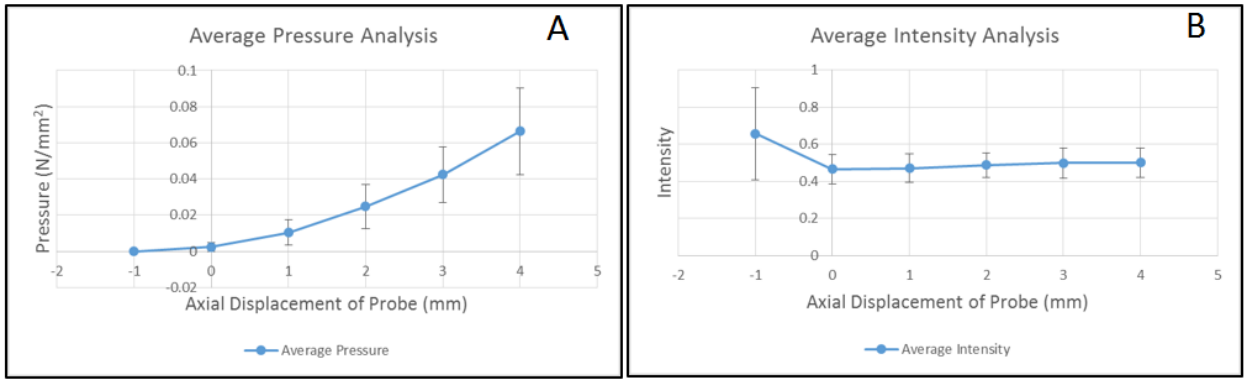

Figure 24: (A) Left graph compares the axial displacement of the optical probe (mm) to the pressure (N/mm^2) applied by the optical probe. (B) Right graphs compares the axial displacement of the optical probe (mm) to the normalized intensity of the reflected light from the LRS system at 630 nm. The two graphs are cross validated to show the correlation between pressure and the normalized intensity of the reflected light from the LRS system.

The average pressure was compared directly to the average intensity to better show the correlation. As a result, as the pressure increases from the initial point of contact from ~0.002 to ~ 0.066 N/mm^2, the intensity changes very slightly, from ~0.46 to ~0.50. This is not a significant change in intensity. Based on this data, pressure does not play a significant role in affecting the intensity of the reflected light intensity from the LRS system.

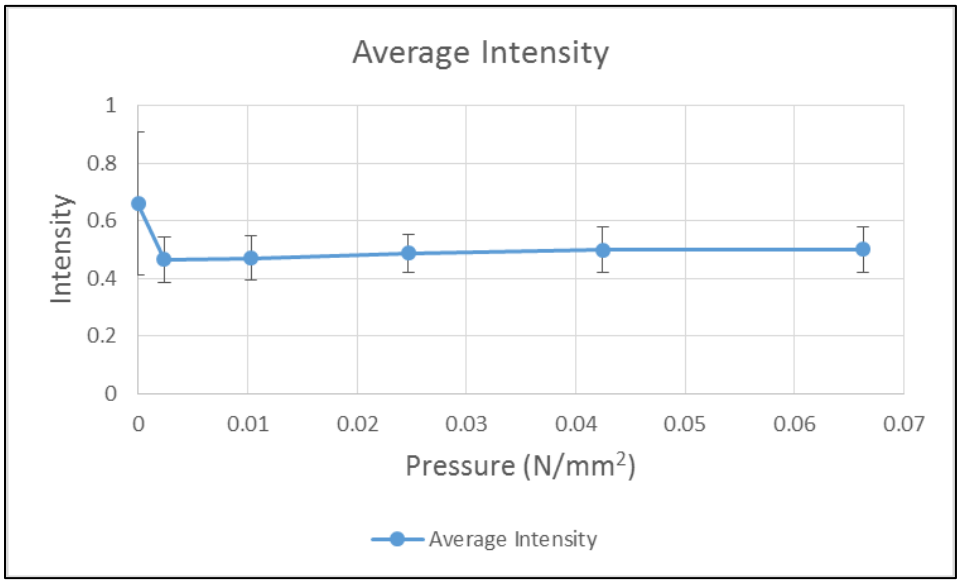

Figure 25: A graph that directly compares the average pressure (N/mm2) to the average intensity at 630 nm of the reflected light measured by the LRS system.

3.8 Penetration Depth Analysis of the New Optical Probes

Referring back to Section 2.5, three optical probes were tested in Intralipid Solution of 0.8% and 1.2%. In the first test, which compares the new 370 µm probe to the old 370 µm probe at 0.8%

Intralipid fluid, both probes had a maximum penetration depth of ~ 1.95 mm at 95% threshold value. In the second test, which compares the new 370 µm probe to the old 370 µm probe at 1.2% Intralipid fluid, both probes had a maximum penetration depth of ~ 1.77 mm at 95% threshold value. Based on these values, the old 370 µm probe and the new 370 µm probe has a range of ~1.77 mm to ~1.95 mm of penetration depth in prostate tissue. The new 370 µm probe can also be confirmed to be just as effective as the old 370 µm probe. This justifies the replacement of the old 370 µm probe with the new 370 µm probe.

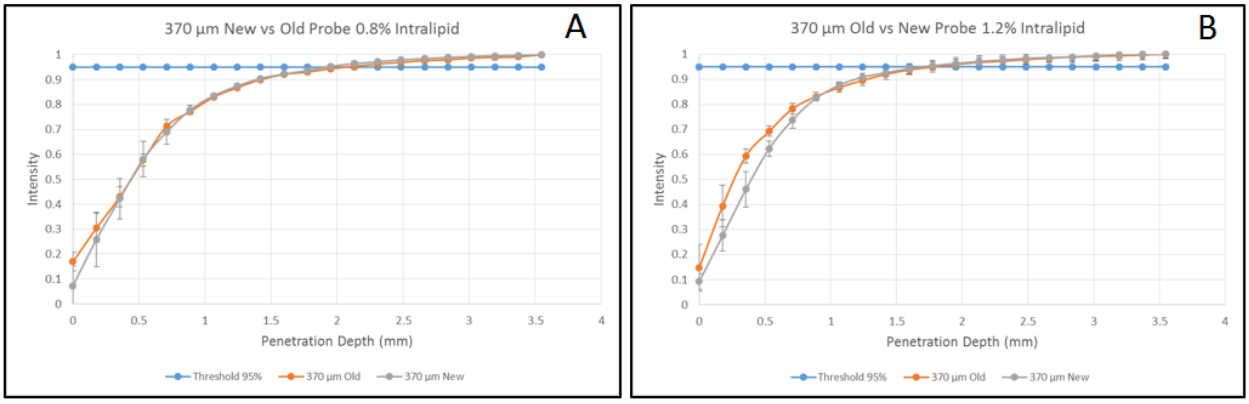

Figure 26: (A) The right graph shows the penetration depth comparison of the intensity of the new 370 µm optical probe to the old 370 µm optical probe in 0.8% Intralipid solution, with a threshold value of 95%. (B) The left graph shows the penetration depth comparison of the intensity the new 370 µm optical probe to the old 370 µm optical probe in 1.2% Intralipid solution, with a threshold value of 95%.

In the next test, the new 370 µm optical probe was compared to the new 125 µm optical probe, to compare the difference in penetration depth associated with a shorter source-detector separation distance. Based off the previous experiment, the penetration depths for the 370 µm optical probe for 0.8% Intralipid solution and 1.2% Intralipid solution were ~1.95 mm and ~1.77 mm, respectively. This is compared to the 125 µm optical probe, which resulted in a penetration depth of ~1.41 mm and ~ 1.06 mm in 0.8% and 1.2% Intralipid solution, respectively. Thus the

new 125 µm optical probe has penetration depth range from ~1.06 mm to ~1.41 mm and is ideal for detecting cancerous tissues more superficial to the outer capsule of the prostate.

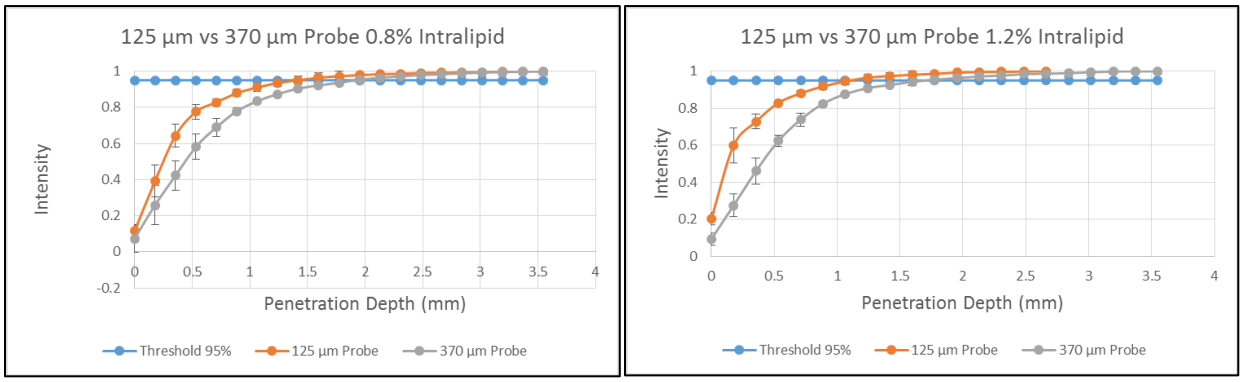

Figure 27: (A) The right graph shows the penetration depth comparison of the intensity of the 125 µm optical probe to the 370 µm optical probe in 0.8% Intralipid solution, with a threshold value of 95%. (B) The left graph shows the penetration depth comparison of the intensity the 125 µm optical probe to the 370 µm optical probe in 1.2% Intralipid solution, with a threshold value of 95%.

3.9 New 2 and 4 Feature Analysis and Results

A statistical two sample t-test was performed on all cancer tissue (GS 6, 3+4, 4+3, and 4+4) on all normal prostate tissue. At a 5% level of significance, it was shown that the wavelengths from ~620 nm to ~780 nm were significant between cancer tissue and normal prostate tissue for the 47 cases of prostate specimen in Henry's study. The wavelengths in this range may prove useful for developing a new 2 Feature or 4 Feature Algorithm, involving only the slopes and intercepts between two or three wavelengths.

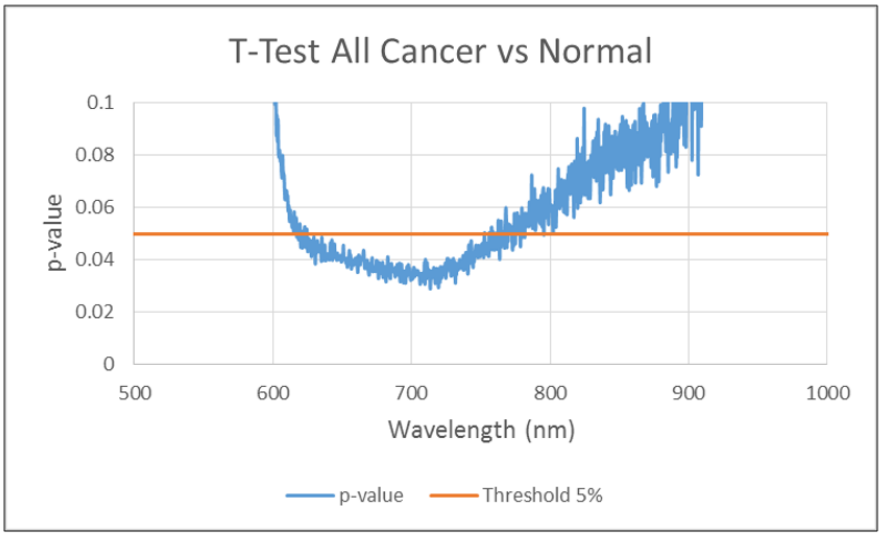

$$t = \frac{(x_1 - x_2)}{\sqrt{\frac{(s_1)^2}{n_1} + \frac{(s_2)^2}{n_2}}}$$

Sample Size:
Cancer: $n_1 = 54$
Normal: $n_2 = 203$

Figure 28: A two sample t-test of the cancer group (GS 6, 3+4, 4+3, 4+4) and the normal prostate tissue group. The sample size of the cancer group is $n_1 = 54$, and the sample size for the normal group is $n_2 = 203$. The range of wavelengths that are found to be significant at a 5% level of significance are from ~620 nm to ~780 nm.

A variety of the 2 or 3 wavelengths were selected, based off of the range from the two sample t-test. (An earlier two sample t-test was ran with a smaller sample size for cancer and normal tissue and the wavelengths from ~610 nm to ~900 nm was found to be significant.) The results were compared to the 5 Feature and 9 Feature algorithm. The three wavelengths of 610-750-900 nm were found to have very similar results to the 5 Feature Algorithm, which is the current "optimal" algorithm. The algorithm was ran on the cancer and normal prostate tissue data and did not take Gleason Score separation into consideration. The 5 Feature Algorithm and the 610-750-900 nm Algorithm were actually tied for the Sen at a value of 0.4444. In addition, the 610-750-900 nm Algorithm had slightly higher values for Spc, PPV, NPV, and Acc testing categories with values of 0.8029, 0.375, 0.8445, and 0.7276, respectively, compared to the 5 Feature Algorithm with values of 0.7980, 0.3692, 0.8437, and 0.7237, respectively. This new three

wavelengths is slightly more effective than the 5 Feature Algorithm and can be utilize for a future potential redesign of the LRS system.

Count	5 feat	9 feat	610-750nm	625-725nm	610-750-850nm	610-750-875nm	610-750-900nm	625-725-825nm	690-750nm	690-750-900nm	690-750-850nm
TP	24	17	21	21	18	23	24	20	21	22	16
FP	41	25	40	41	33	35	40	35	43	35	29
TN	162	178	163	162	170	168	163	168	160	168	174
FN	30	37	33	33	36	31	30	34	33	32	38
Total	257	257	257	257	257	257	257	257	257	257	257
Cancer	54	54	54	54	54	54	54	54	54	54	54
Normal	203	203	203	203	203	203	203	203	203	203	203
Sen	**0.44444**	0.31481	0.388888889	0.38888889	0.333333333	0.425925926	**0.444444444**	0.37037037	0.388888889	0.407407407	0.296296296
Spc	0.79803	**0.87685**	0.802955665	0.79802956	0.837438424	0.827586207	0.802955665	0.827586207	0.78817734	0.827586207	0.857142857
PPV	0.36923	**0.40476**	0.344262295	0.33870968	0.352941176	0.396551724	0.375	0.363636364	0.328125	0.385964912	0.355555556
NPV	0.84375	0.82791	0.831632653	0.83076923	0.825242718	0.844221106	**0.844559585**	0.831683168	0.829015544	0.84	0.820754717
Acc	0.72374	**0.75875**	0.715953307	0.71206226	0.73151751	0.743190661	0.727626459	0.73151751	0.704280156	0.739299611	0.739299611

Figure 29: A chart comparing the different combinations of 2 or 3 wavelengths, within the range of 610 nm to 900 nm. The slope and intercept were calculated between the 2 or 3 wavelengths to form the 2 or 4 Feature Algorithm. The results were compared to the 5 Feature Algorithm and the 9 Feature Algorithm. The 5 Feature Algorithm and 610-750-900nm Algorithm had the highest value for Sen, The 610-750-900nm had the highest value for NPV, and the 9 Feature Algorithm had the highest value for Spc, PPV, and Acc.

Chapter 4: Discussion

4.1 Gleason Score Discussion

The Gleason Score plays a very important role in terms of LRS cancer classification. Based on previous work, Lay, *et al.* [19] They found that LRS is not very effective in terms of distinguishing between normal tissue and GS 6 (or 3+3). Gleason Score of 6 is essentially made up almost entirely of Gleason Grade 3, which has similar optical properties to that of normal prostate tissue and the cells are well differentiated, similar to normal prostate tissue. In addition, Gleason Grade 3 is not considered as an aggressive form of cancer and are less likely to spread beyond the prostate in a metastatic manner. Essentially, GS 6 is considered a low risk form of cancer.

A Gleason Score of 3+4 or 4+3 is determined by the volume of Gleason Grade 4 that is present in the cancerous tissue. If there is less than 50% volume of Gleason Grade 4, then the case is classified as a GS 3+4, and if there is more than 50% volume of Gleason Grade 4, then the case is classified as a GS 4+3. Gleason Grade 4 is considered an aggressive form of the cancer and highly likely to exhibit metastatic characteristics.

In the GS class of 3+4, there is a higher volume of the Gleason Grade 3. As mentioned before, this is a very low risk form of cancer and is highly unlikely to exhibit malignant characteristics. Although GS 3+4 is more aggressive than GS 6, GS 3+4 is still considered a non-aggressive form of cancer due to the higher volume of Gleason Grade 3.

During the LRS measurement results from Section 3.5, GS 6 and GS 3+4 cases were found to have very similar optical properties and peak intensity levels. These similar readings may be attributed

to the LRS measurement location to be on a Gleason Grade 3 location of the tumor. In a GS 6 case, there is a 100% chance of measuring a Gleason Grade 3 location, and in a GS 3+4 case, there is at least a 50% chance of measuring a Gleason Grade 3 location. This may in fact be the cause behind the low intensity LRS readings of the GS 3+4 cases. In the future, the pathologist must record the Gleason Grade at the location of the LRS measurement spot for further validation.

The intensity levels of both GS 6 and GS 3+4 were found to be low, and almost similar to the spectral readings from normal prostate tissue. While the GS of 4+3 and 4+4 were found to have an obvious spectral difference and higher peak intensity compared to the normal, GS 6, and GS 3+4 groups. Thus it may be wise to group the dataset into a binary fashion, of high risk groups (GS 4+3 and 4+4) versus low risk groups (normal, GS 6, GS 3+4).

In addition, the total dataset is highly bias to the Group 2 (GS 3+4), with 173 total measurements (combined cancer and normal readings). Group 1 (GS 6) only has 24 total measurements, Group 3 (GS 4+3) has a total of 22 total measurements, and Group 4 (GS 4+4) has a total of 38 measurements. It is recommended to obtain more readings belonging to Groups 1, 3, and 4 to create a more balanced dataset.

4.2 5 Feature and 9 Feature Discussion

Both 5 Feature and 9 Feature algorithms were ran on the same set of testing data. Based on the results from Section 3.6, the 5 Feature algorithm was found to be superior to the 9 Feature algorithm in terms of sensitivity. In the Gleason Group 4, the 5 Feature Algorithm had the highest sensitivity value of 72.70%, compared to the much lower 9 Feature Algorithm value of 54.5%. Both algorithms did not have high values for sensitivity for Gleason Groups 1, 2 or 3 with values

of 50%, 40.7%, and 42.90%, respectively for the 5 Feature Algorithm; and 50%, 29.6%, and 28.6%, respectively for the 9 Feature Algorithm. This may be attributed to the LRS measurement spot on a Gleason Grade 3 location. This shows that The 5 Feature Algorithm is effective, but not perfect, in terms of detection of high grade cancer positive readings, which is essential for the future steps in real-time positive margin detection. The 9 Feature Algorithm consistently had higher values for Specificity, which may be attributed to the much higher sample size of normal prostate tissue readings. In Gleason Group 3, both 5 Feature and 9 Feature Algorithms had an equal Specificity value of 93.3%, but in Gleason Group 4, the 9 Feature Algorithm had a higher Specificity value of 88.90%, compared to the 5 Feature Algorithm value of 81.5%, which is also an acceptable value. But having acceptably high values in both sensitivity and specificity is important for positive margin detection, thus the 5 Feature Algorithm will serve as the current optimal algorithm to be used in future studies.

4.3 Pressure Analysis Discussion

Referring back to Figure 25, from Section 3.7, at -1 mm, which is 1 mm above the surface of the prostate, the intensity is slightly higher, compared to the rest of the graph. This is due to the reflected light that fails to penetrate the prostate tissue, and the larger amount of the light is reflected and detected by the LRS probe. But as soon as the probe makes initial surface contact with the prostate tissue, at 0 mm, the light intensity stabilizes. After each increment of axial displacement of the probe, the light intensity does not vary too much, up to 4 mm of axial displacement. This implies that the surgeon must have secure contact of the optical probe to the surface of the prostate tissue to ensure proper LRS measurements. Thus, according to Figure 25,

the pressure applied by the optical probe does not play a significant role in affecting the spectral reading of the LRS probe.

4.4 Penetration Depth of the New Optical Probes Discussion

During the penetration depth analysis of the new optical probes from Section 3.8, it was found that both 370 µm probe had a penetration depth range from ~ 1.77 mm to ~ 1.95 mm in Intraplipid solution and 125 µm probe had a penetration depth range from ~1.06 mm to ~ 1.41 mm. In the current LRS measurements, the 370 µm probe has been the primary tool used for detection of positive surgical margins of prostate cancer. But the clinicians are most interested in the cases where the cancer has spread extremely close or beyond the margin of the prostate capsule. The current 370 µm probe has a maximum penetration depth of ~1.95 mm, but making a transition to the new 125 µm probe, it would filter out many LRS cancer positive readings that were previously detected by the 370 µm probe between ~1.41 mm to ~1.95 mm of depth. This would allow more focus on the cancers that are closer to the outer capsule, up to ~1.41 mm of depth, which are at a higher risk for a positive margins. This would reduce the number of false positives margins and reduce the need to remove the excess surrounding tissues and nerves. In conclusion, with the current 370 µm probe, tumors within ~1.95 mm to the margins may require removal of the surrounding tissues, but with the new 125 µm probe, tumors within ~1.41 mm may require removal of the surround tissue. This may allow more nerve-sparring operations during a prostatectomy and help maintain the erectile nervous functions of the patient.

4.5 Potential Future Study Using an Light-Emitting Diode (LED) System and the 2/4 Feature Approach

Referring back to Section 3.9, 2 and 4 Features were chosen based off the statistical two sample t-test. And the wavelengths of 610-750-900 nm were found to have similar results to the optimal 5 Feature Algorithm in terms of Sen, Spc, PPV, NPV and Acc. This may pave a new direction for remodeling the LRS system into a cost efficient manner for potential commercialization. The currently LRS system costs approximately $5000 to produce, but switching to an LED system would greatly reduce costs to $500 - $800.

The basic concept behind the LED system would require three LEDs that emits at 610 nm, 750 nm, and 900 nm. This is opposed to the LRS system that emits a broadband wavelength from ~465 - ~ 1140 nm. The intensity values can be recorded at each LED wavelength value, and the slope and y-intercept can be calculated between each wavelength. Thus the 4 Features can be extracted from the 610-750-900 nm Algorithm for cancer classification.

4.6 New Algorithm Developed by Rahilsadat Hosseini

A new algorithm was developed by a PhD Candidate, Rahilsadat Hosseini, from the Industrial & Systems Engineering Department at the University of Texas at Arlington. In her work she, she developed an effective cancer classification model that uses support vector machine for classification of normal prostate tissue class, middle grade (GS 3+4) class, and high grade (GS 4+3 and 4+4) cancer class, using ensemble of trees. Her data is based on an earlier set of collected data, with 155 normal and 29 cancerous readings. In her current progress, she used the concept

of moving window in order to define a range of wavelengths that are optimal for cancer classification.

With the multi-three class system, she has approximately 60-62% accuracy for each class using ensemble of Trees algorithm. If she uses a two class system, that considers only the normal class versus the high grade cancer class (GS 4+3 and 4+4), she has a Sensitivity of 100% and a Specificity of ~83%. If she splits the two classes into the normal class versus all cancer class (GS 3+4, 4+3, and 4+4), she has a Sensitivity of 75% and Specificity of 77.5%. The results are much improved compared to the current algorithms. This new algorithmic approach could potentially become an alternative to the current 5 Feature Algorithm.

4.7 Limitations and Future Improvements

The primary limitation to the study involves the Gleason Grade at the location of the measurement spot. Currently, only the pre-operative Gleason Score information are known from the biopsy reports. In addition, this pre-operative Gleason Score information represents the entire prostate, and not a specific location of the prostate. It is vital to obtain the Gleason Grade at each measurement spot in order to properly validate the effectiveness of the LRS system and the 5/9 Feature Algorithm. In the current study, there are a much higher number of cases in the GS 3+4 category, compared to all other GS categories. Thus the data is highly biased towards the GS 3+4 data. In a GS 3+4 case, the LRS measurements has a much higher possibility of being made on Gleason Grade 3 location, rather than a Gleason Grade 4 location. From previous studies, it was confirmed that LRS was ineffective for GS 6, which is comprised primarily of Gleason Grade 3. This may have greatly affected the Sen, Spc, PPV, NPV, and Acc during the 5/9

Feature Algorithm analysis. As Dr. Jeffrey Cadeddu says, “We are setting ourselves up to fail.” Thus, in future studies, the pathologist must record information on the Gleason Grade at the spot of the LRS measurement for proper validation of the LRS system.

In the current study, there are 32 prostate cases in the GS 3+4 category, compared to the GS 4+3 and GS 4+4 with only 4 and 7 cases, respectively. The data is high imbalanced and biased towards the GS 3+4 category. In order to counter this, there must be more LRS cases from the GS 4+3 and GS 4+4 categories to create a more balanced dataset.

Also, the current LRS system measures the surface of the prostate in a point by point measurement pattern with a detection diameter of only 370 µm. Measuring the entire surface of the prostate would be extremely time consuming and would be inefficient in real time during surgery. Creating an array of optical probes, in an effort to measure a larger surface area and reducing time, would be very costly.

References

1. Hoffman, Matthew. "Picture of the Prostate." *WebMD*. WebMD, n.d. Web. 27 Mar. 2017.
2. "What Is Prostate Cancer?" *American Cancer Society*. N.p., n.d. Web. 27 Mar. 2017.
3. "Key Statistics for Prostate Cancer | Prostate Cancer Facts." *American Cancer Society*. N.p., n.d. Web. 21 Apr. 2017.
4. "Treatment Options." Prostate Cancer Foundation, 2017. Web. 27 Mar. 2017.
5. "What is Active Surveillance?" Prostate Cancer Foundation, 2017. Web. 27 Mar. 2017.
6. "Radiation Therapy" Prostate Cancer Foundation, 2017. Web. 28 Mar. 2017.
7. "Prostatectomy Surgery" Prostate Cancer Foundation, 2017. Web. 28 Mar. 2017.
8. Beard, Clair J., Elizabeth M. Genega, Andrew A. Wagner, and Marc B. Garnick. "Positive Surgical Margins Following Radical Prostatectomy." Harvard University, 2017. Web. 28 Mar. 2017.
9. Jacques, Steven L. "Optical properties of biological tissues: a review." *IOP Publishing, Physics in Medicine and Biology* (2013): R37-61. Web. 25 Mar. 2017.
10. Van Staveren, Hugo J., Christian J. M. Moes, Jan Van Marle, Scott A. Prahl, and Martin J. C. Van Gemert. "Light scattering in Intralipid-10% in the wavelength range of 400-1100 nm." *Applied Optics* (1991): 4507-514. Web. 24 Mar. 2017.
11. Zijlstra, W.G., Buursma, A. & Assendelft, O.W. Visible and Near-infrared Absorption Spectra of Human and Animal Hemoglobin: Determination and Application (VSP: 2000).
12. Montironi, Rodolfo, Antonio Lopez Beltran, Roberta Mazzucchelli, Liang Cheng, and Marina Scarpelli. "Handling of Radical Prostatectomy Specimens: Total Embedding with Large-Format Histology." *Hindawi Publishing Corporation, International Journal of Breast Cancer* (2012): n. pag. Web. 23 Mar. 2017.
13. Zonios, George, and Aikaterini Dimon. "Modeling diffuse reflectance from semi-infinite turbid media: application to the study of skin optical properties." *Optical Society of America* (2006): 8661-674. Web. 12 Apr. 2017.
14. Wang, Xinlong, Monica Morgan, Payal Kapur, Jeffrey Cadeddu, Claus R. Roehrborn, and Hanli Liu. "Light Scattering Serves as Optical Signature for Detection of Positive Surgical Margins on prostate capsule." *OSA* (2014): n. pag. Web. 12 Feb. 2017.
15. Morgan, Monica S. C., Aaron H. Lay, Xinlong Wang, Payal Kapur, Asim Ozayar, Maryam Sayah, Li Zeng, Hanli Liu, Claus G. Roehrborn, and Jeffrey A. Cadeddu. "Light Reflectance Spectroscopy to Detect Positive Surgical Margins on Prostate Cancer Specimens." *New Technology and Techniques, American Urological Association Education and Research, Inc.* 195 (2016): 479-84. Web.
16. Fawcett, Tom. "An Introduction to ROC Analysis." *Pattern Recognition Letters* 27.8 (2006): 861-74. Web. 12 Mar. 2017.
17. Powers, David M W. "Evaluation: From Precision, Recall and F-Measure to ROC, Informedness, Markedness & Correlation." *Journal of Machine Learning Technologies* 2.1 (2011): 37-63. Web. 23 Mar. 2017.
18. Sharma, Vikrant. "A Novel Minimally Invasive Dual-Modality Fiber Optic Probe For Prostate Cancer Detection." *The University of Texas at Arlington, PhD Dissertation* (2012): Web. 14 Apr. 2017.
19. Lay, Aaron, Monica Morgan, Xinlong Wang, Payal Kapur, Hanli Liu, Claus Roehrborn, and Jeffrey Cadeddu. "Detecting Positive Surgical Margins: Utilization of Light Reflectance Spectroscopy on

ex vivo Prostate Specimens." *Department of Urology, University of Texas Southwestern Medical Center: Web.* 23 Apr. 2017.

Appendix A

5/9/4 Feature Algorithm LRS Results with Pathology Results

Measurement Point Identification (ID)	Abbreviation
Left Lateral of Prostate	L
Right Lateral of Prostate	R
Apex Region of Prostate	A
Base Region of Prostate	B
Green Ink	G
Yellow Ink	Y
Red Ink	R
Purple Ink	P

*The numerical portion of the measurement point ID represents the number of the prostate case that was measured.

LRS 5/9/4 Feature Diagnosis	LRS Output
LRS Cancer Negative	0
LRS Cancer Positive	1

Pathology Report "Truth Value"	Pathology Output
Pathology Negative Margin - Normal Tissue	0
Pathology Positive Margin – Cancer at Margin	1
Pathology Negative Margin – Cancer Near Margin*	2

*For pathology output '2', a pathology comment is provided for the depth of the cancerous tumor from the surface of the prostate capsule margin, in millimeters.

Measurement Point ID	5 Feature	9 Feature	4 Feature (610-750-900 nm)	Pathology	Pathology Comments	Gleason Score
3 LG	1	1	1	2	3mm	3+4
3 LP	0	0	0	2	1mm	3+4
3 LY	1	1	1	0		3+4
3 RG	0	0	0	0		3+4
3 RP	0	0	0	0		3+4
3 RY	0	0	0	0		3+4
4 LG	0	0	0	0		4+4
4 LP	0	0	0	0		4+4
4 LY	1	1	1	0		4+4
4 RG	0	0	0	0		4+4
4 RP	0	0	0	0		4+4
4 RY	0	0	0	0		4+4
5 LG	0	0	0	0		4+4
5 LP	0	0	0	0		4+4
5 LYA	0	0	0	0		4+4
5 LYB	1	0	1	2	4mm	4+4
5 RG	1	1	1	2	0.5mm	4+4
5 RP	0	0	0	0		4+4
5 RYA	1	1	1	2	1mm	4+4
5 RYB	1	1	1	2	0.5mm	4+4
6 LG	0	0	0	0		3+4
6 LP	0	0	0	0		3+4
6 LYA	0	0	0	0		3+4
6 LYB	1	0	1	0		3+4
6 RG	0	0	0	2	0.6mm	3+4
6 RP	0	0	0	2	0.5 mm	3+4
6 RYA	0	0	0	2	0.5mm	3+4
6 RYB	0	0	0	2	0.6mm	3+4
7 LG	0	1	0	2	2mm	3+4
7 LP	0	0	0	0		3+4
7 LY	0	0	0	0		3+4
7 RG	1	0	1	0		3+4
7 RP	1	0	1	0		3+4
7 RY	0	0	0	0		3+4
9 LG	0	0	0	0		3+3
9 LP	0	0	0	0		3+3
9 LY	0	0	0	0		3+3
9 RG	0	0	0	0		3+3
9 RP	0	0	0	0		3+3
9 RY	0	0	0	2	0.5mm	3+3
10 LG	0	0	0	0		3+4

10 LP	0	0	0	0		3+4
10 LY	0	1	0	0		3+4
10 RG	0	0	0	0		3+4
10 RP	0	0	0	0		3+4
10 RY	0	0	0	0		3+4
11 LG	0	0	0	2	4mm	3+4
11 LP	0	0	0	0		3+4
11 LYA	0	0	0	0		3+4
11 RG	1	1	0	0		3+4
11 RP	0	0	0	0		3+4
11 RYA	0	0	0	0		3+4
11 RYB	0	0	0	0		3+4
12 LY	0	0	0	0		3+4
12 RG	1	0	1	0		3+4
12 RP	1	1	1	0		3+4
12 RY	0	0	0	0		3+4
14 LG	0	0	0	0		3+4
14 LP	0	0	0	0		3+4
14 LY	1	1	1	2	0.75mm	3+4
14 RG	0	0	0	0		3+4
14 RP	0	0	0	0		3+4
14 RY	0	0	0	0		3+4
15 LG	0	0	0	2	2mm	3+4
15 LP	1	0	1	2	2mm	3+4
15 LY	0	0	0	0		3+4
15 RG	0	0	0	0		3+4
15 RP	0	0	0	0		3+4
15 RY	1	0	1	0		3+4
17 LG	0	0	0	2	1mm	3+4
17 LP	0	1	0	2	1.5mm	3+4
17 LYB	0	0	0	0		3+4
17 RG	0	0	0	0		3+4
17 RP	0	0	0	0		3+4
17 RYA	0	0	0	0		3+4
17 RYB	0	0	0	0		3+4
18 LG	0	0	0	0		3+4
18 LYB	0	0	0	0		3+4
18 RG	0	0	0	0		3+4
18 RP	0	0	0	0		3+4
18 RYA	0	0	0	0		3+4
20 LYA	0	0	0	0		3+4
20 RG	1	0	0	0		3+4
20 RP	0	0	0	0		3+4

20 RY	0	0	0	0		3+4
22 LG	1	0	1	2	1mm	4+4
22 LYA	1	1	1	2	0.5mm	4+4
22 RG	1	0	1	0		4+4
22 RYA	0	0	0	0		4+4
23 LG	0	0	0	0		3+4
23 LP	0	0	0	0		3+4
23 LYA	0	0	0	0		3+4
23 LYB	0	0	0	0		3+4
23 RG	0	0	0	0		3+4
23 RP	0	0	0	0		3+4
23 RYA	0	0	0	0		3+4
24 LG	0	0	0	0		4+4
24 LP	0	0	0	0		4+4
24 LYA	0	0	0	0		4+4
24 RG	0	0	0	0		4+4
24 RP	0	0	0	0		4+4
24 RYA	0	0	0	0		4+4
25 LG	0	0	0	0		3+4
25 LYA	0	0	0	0		3+4
25 RG	0	0	0	2	0.01mm	3+4
25 RP	0	0	0	2	0.01mm	3+4
25 RYA	1	0	1	2	0.25mm	3+4
26 LG	0	0	1	0		4+3
26 LP	0	0	0	0		4+3
26 LYA	0	0	0	0		4+3
26 RG	0	0	0	0		4+3
26 RP	0	0	0	0		4+3
26 RYA	0	0	0	0		4+3
27 LG	1	1	1	0		3+4
27 LP	0	0	0	0		3+4
27 LY	0	0	0	0		3+4
28 LG	0	0	0	0		3+4
28 LP	0	0	0	2	0.5mm	3+4
28 RG	1	1	1	0		3+4
28 RP	1	1	1	2	4mm	3+4
28 RYA	0	0	0	0		3+4
29 LYA	0	0	0	0		4+3
29 LYB	1	1	1	1		4+3
29 RG	0	0	0	0		4+3
29 RYA	0	0	0	0		4+3
30 RG	0	0	0	0		3+4
30 RP	0	0	0	0		3+4

31 LP	0	0	0	0		3+3
31 LY	1	1	1	2	5mm	3+3
31 RG	1	0	1	0		3+3
31 RP	1	0	1	0		3+3
32 LG	1	0	1	0		3+4
32 LYA	0	0	0	0		3+4
32 RG	1	1	1	0		3+4
32 RP	1	1	1	0		3+4
32 RYA	0	0	0	0		3+4
33 LG	0	0	0	0		3+4
33 RG	1	1	1	0		3+4
33 RP	1	1	1	0		3+4
34 LP	0	0	0	0		3+4
34 LYA	0	0	0	0		3+4
34 RG	1	1	1	0		3+4
34 RP	0	0	0	0		3+4
35 LG	0	0	0	0		3+4
35 LYA	0	0	0	0		3+4
35 LYB	0	0	0	0		3+4
35 RYB	1	0	1	0		3+4
36 LG	0	0	0	0		3+4
36 LP	0	0	0	0		3+4
36 LYA	0	0	0	0		3+4
36 LYB	0	0	0	0		3+4
36 RP	0	0	0	0		3+4
36 RYA	0	0	0	0		3+4
37 LP	0	0	0	0		4+4
37 LYB	1	1	1	2	3mm	4+4
37 RG	1	0	1	2	1.5mm	4+4
37 RP	1	1	1	2	1mm	4+4
37 RYB	1	1	1	0		4+4
38 LG	0	0	0	2	0.5mm	3+4
38 LP	0	0	0	0		3+4
38 RG	0	0	0	2	2mm	3+4
38 RP	1	1	1	0		3+4
38 RY	0	0	0	0		3+4
39 LG	0	0	0	0		3+4
39 LP	0	0	0	0		3+4
39 LY	1	0	0	0		3+4
39 RG	1	1	1	0		3+4
39 RY	0	0	0	0		3+4
40 LG	0	0	0	0		3+4
40 LP	0	0	0	0		3+4

40 RG	1	0	1	0		3+4
40 RP	0	0	0	0		3+4
41 LG	0	0	1	0		3+4
41 LP	1	0	1	0		3+4
41 LYA	0	0	0	0		3+4
41 LYB	1	0	1	0		3+4
41 RG	0	0	0	2	3mm	3+4
41 RP	0	0	0	0		3+4
41 RYA	0	0	0	0		3+4
41 RYB	0	0	0	0		3+4
42 LG	0	0	0	0		3+4
42 LP	0	0	0	0		3+4
42 LY	1	1	1	0		3+4
42 RG	1	1	1	2	2mm	3+4
42 RP	0	0	0	0		3+4
42 RY	0	0	0	0		3+4
43 LG	0	0	0	0		3+4
43 LP	0	0	0	0		3+4
43 LY	1	1	1	2	0.1mm	3+4
43 RG	0	0	0	0		3+4
43 RP	0	0	0	0		3+4
43 RY	1	1	1	0		3+4
44 LG	0	0	0	0		4+4
44 LR	1	0	0	1		4+4
44 LY	1	0	1	0		4+4
44 RG	0	0	0	0		4+4
44 RR	0	0	0	0		4+4
44 RY	0	0	0	0		4+4
45 LG	1	1	1	0		3+3
45 LR	0	0	0	0		3+3
45 LYA	0	0	0	0		3+3
45 LYB	1	1	1	0		3+3
45 RG	1	1	1	0		3+3
45 RR	1	0	1	0		3+3
45 RYA	0	0	0	0		3+3
45 RYB	1	1	1	0		3+3
46 LG	0	0	0	2	0.5mm to deeper tumor	4+3
46 LR	0	0	0	2	1mm to deeper tumor	4+3
46 LY	1	1	1	2	1.5 mm	4+3
46 RG	0	0	0	0		4+3
46 RR	0	0	0	0		4+3
46 RY	1	1	1	0		4+3
47 LG	0	0	1	2	0.5mm	3+4

47 LR	0	0	0	2	0.4mm	3+4
47 LY	1	0	1	2	1mm to tumor	3+4
47 RG	1	1	1	0		3+4
47 RR	0	0	0	0		3+4
47 RY	1	1	1	0		3+4
48 LG	0	0	0	0		3+4
48 LR	0	0	0	0		3+4
48 LY	0	0	0	0		3+4
48 RG	0	0	0	0		3+4
48 RR	0	0	0	0		3+4
48 RY	0	0	0	0		3+4
49 LG	0	0	0	2	2mm	4+4
49 LR	0	0	0	2	2mm to tumor	4+4
49 LYA	0	0	0	2	2mm	4+4
49 LYB	1	1	1	2	2mm	4+4
49 RR	0	0	0	0		4+4
49 RYA	0	0	0	0		4+4
49 RYB	1	1	1	0		4+4
50 LG	0	0	0	2	3mm	3+4
50 LR	0	0	0	0		3+4
50 LY	0	0	0	0		3+4
50 RG	0	0	0	0		3+4
50 RR	0	0	0	0		3+4
50 RY	0	0	0	0		3+4
51 LG	0	0	1	0		3+3
51 LR	0	0	0	0		3+3
51 LY	0	0	0	0		3+3
51 RG	0	0	0	0		3+3
51 RR	0	0	0	0		3+3
51 RY	0	0	0	0		3+3
52 LG	0	0	0	0		3+4
52 LR	0	0	0	2	not visualized (0.5mm deep)	3+4
52 LYA	0	0	0	0		3+4
52 LYB	0	0	0	2	1 mm to tumor	3+4
52 RG	0	0	0	2	not visualized (1mm)	3+4
52 RR	0	0	0	2	0.7mm to tumor	3+4
52 RYA	0	0	0	0		3+4
52 RYB	1	0	1	2	0.8mm to tumor	3+4
53 LG	0	0	0	0		4+3
53 LR	0	0	0	0		4+3
53 LY	0	0	0	0		4+3
53 RG	0	0	0	2	1.5 mm deep tumor 4+4	4+3

53 RR	0	0	0	2	0.8 mm to tumor	4+3
53 RY	1	0	1	2	1.5 mm deep tumor 4+4	4+3